Improved base editing and functional screening in *Leishmania* via co-expression of the AsCas12a ultra variant, a T7 RNA Polymerase, and a cytosine base editor

Nicole Herrmann May[1], Ngoc Anh Cao[1], Annika Schmid[1], Fabian Link[1,2], Jorge Arias-del-Angel[1,2], Elisabeth Meiser[1] and Tom Beneke[1,*]

[1] Department of Cell and Developmental Biology, Biocentre, University of Würzburg, Am Hubland, 97074 Würzburg, Germany

[2] Division of Immunology, Paul-Ehrlich-Institut, Langen, Germany.

* To whom correspondence should be addressed. Email: tom.beneke@uni-wuerzburg.de

ABSTRACT

The ability to analyse the function of all genes in a genome is highly desirable, yet challenging in *Leishmania* due to a repetitive genome, limited DNA repair mechanisms and lack of RNA interference in most species. While our introduction of a cytosine base editor (CBE) demonstrated potential to overcome these limitations (Engstler and Beneke (2023)), challenges remained, including low transfection efficiency, variable editing rates across species, parasite growth effects, and competition between deleterious and non-deleterious mutations. Here, we present an optimized approach addressing these issues.

We identified a T7 RNAP promoter variant ensuring high editing rates across *Leishmania* species without compromising growth. A revised CBE single-guide RNAs (sgRNAs) scoring system was developed to prioritize STOP codon generation. Additionally, a triple-expression construct was created for stable integration of CBE sgRNA expression cassettes into a *Leishmania* safe harbor locus using AsCas12a ultra-mediated DNA double-strand breaks, increasing transfection efficiency by ~400-fold to one transfectant per 70 transfected cells. Using this improved system for a small-scale proof-of-principle pooled screen, we successfully confirmed the essential and fitness-associated functions of CK1.2, CRK2, CRK3, AUK1/AIRK, TOR1, IFT88, IFT139, IFT140 and RAB5A in *L. mexicana*, demonstrating a significant improvement over our previous method. Lastly, we show the utility of co-expressing AsCas12a ultra, T7 RNAP and CBE for hybrid CRISPR gene replacement and base editing within the same cell line.

Overall, these improvements will broaden the range of possible gene editing applications in *Leishmania* species and will enable a variety of loss-of-function screens in the near future.

32 **INTRODUCTION**

33 CRISPR/Cas9 gene editing has greatly improved loss-of-function experiments in *Leishmania*, and
34 bar-seq screens, which involve individually deleting, barcoding, and pooling mutants for analysis,
35 have facilitated the functional dissection of large gene cohorts (Baker et al., 2021; Beneke et al., 2019;
36 Beneke and Gluenz, 2019; Beneke and Gluenz, 2020; Beneke et al., 2017; Burge et al., 2020;
37 Damianou et al., 2020). However, the applications of bar-seq screens are limited, and it remains
38 difficult to target the vast *Leishmania* repertoire of repetitive genetic elements by gene replacement
39 approaches. In addition, *Leishmania* parasites lack crucial components of the non-homologous DNA
40 end joining (NHEJ) pathway (Passos-Silva et al., 2010; Zhang et al., 2022). As a result, CRISPR-
41 induced DNA double-strand breaks (DSB) lead to unpredictable DNA deletions, increased cell death
42 during DNA repair failures, prolonged repair times and generally low editing rates (Zhang et al., 2017;
43 Zhang and Matlashewski, 2015; Zhang and Matlashewski, 2019; Zhang et al., 2022). Without other
44 means of selection, such as the selection of drug resistance-associated edits, this complicates further
45 the targeting of dispersed multi-copy genes and applications of pooled CRISPR transfection formats.
46 While RNA interference (RNAi) could offer an alternative (de Paiva et al., 2015; Lye et al., 2022), its
47 use is confined to species within the *Viannia* subgenus, restricting its applicability in the majority of
48 *Leishmania* species (Lye et al., 2010; Ullu et al., 2004).

49 We have recently shown how the use of the hyBE4max cytosine base editor (CBE) (Zhang et al.,
50 2020) could potentially overcome these limitations. We demonstrated how the conversion of cytosine
51 to thymine, and thereby the introduction of STOP codons, enables the functional disruption of single-
52 and multi-copy genes in *Leishmania* species without requiring DSB, homologous recombination, the
53 additional use of donor DNA, or isolation of clones (Engstler and Beneke, 2023). Importantly, we
54 presented how this method can be used to identify essential genes in pooled loss-of-function screens
55 via the delivery of plasmid libraries, thereby providing a proof-of-principle experiment for how large-
56 scale pooled CRISPR transfection fitness screens could be carried out in *Leishmania*. However, we
57 also highlighted the need for additional improvements of our method (Engstler and Beneke, 2023).

58 For example, since we used a ribosomal promoter derived from *L. donovani* for expression of the
59 CBE and single guide RNA (sgRNA), editing efficiencies varied greatly between species, and for
60 some *Leishmania* parasites, sufficient editing could be only achieved after weeks in culture. Our
61 attempts to use different promoters, such as the T7 RNA Polymerase (RNAP) promoter were
62 unsuccessful, as their employment for CBE sgRNA expression resulted in strong growth defects.
63 Furthermore, the transfection of pooled plasmid libraries led to combinatorial knockout effects, with
64 approximately one-third of all transfectants harbouring more than one CBE-sgRNA expression
65 plasmid. In addition, the transfection efficiency of plasmid pools was generally low, yielding only ~1
66 transfectant out of 30,000 transfected cells. To compensate for combinatorial effects and the relatively
67 low transfection rate, a large number of cells would need to be transfected to enable large-scale
68 pooled CRISPR transfection screens. Lastly, we noticed that non-deleterious mutations within the
69 CBE editing window can become dominant over desired mutations, especially when targeting
70 essential or growth-affecting genes.

Here, we aimed to develop our base editing approach further and deliver needed improvements. We show how we have identified a T7 RNAP promoter variant that enables stable expression of CBE sgRNAs and results in high editing rates within a short period of time without having significant effects on parasite growth. In addition, we present a construct that allows to express not only T7 RNAP and the hyBE4max CBE but also a highly efficient variant of a Cas12a nuclease derived from *Acidaminococcus sp.* (AsCas12a ultra (Zhang et al., 2021), formerly AsCpf1). Using AsCas12a ultra-mediated DSBs, we have developed a novel approach to deliver and integrate CBE sgRNA expression cassettes into the *Leishmania* 18S rRNA safe harbor locus (Misslitz et al., 2000; Sorensen et al., 2003). We present evidence that the integration of these expression cassettes is precise at the target locus and we demonstrate that this approach has increased transfection rates by up to 400-fold. Using this improved CRISPR tool, we conducted a small-scale loss-of-function screen in *L. mexicana*, targeting nine known essential genes with 24 CBE sgRNAs and 15 non-targeting control sgRNAs. This approach successfully detected all growth-associated phenotypes in a pooled screening format. In a final optimisation step, we have also improved our CBE sgRNA design and scoring tool, www.leishbaseedit.net, to prioritize sgRNAs with fewer theoretical risks of generating edits that do not result in a STOP codon. We believe that these optimisation steps now enable us to deliver a range of gene editing applications, including large-scale loss-of-function screens, in *Leishmania* species without limitations due to extreme cases of gene copy numbers, aneuploidy and/or lack of RNAi components.

RESULTS and DISCUSSION

T7 RNAP promoter variant-driven CBE sgRNA expression reduces toxicity and improves editing efficiency

In our first version of a CBE toolbox for *Leishmania* we utilized a ribosomal promoter derived from *L. donovani* for CBE protein and sgRNA expression. While achieving high editing rates with this single plasmid system (Figure 1A) (Engstler and Beneke, 2023), efficiencies varied greatly among species, requiring for example over 40 days of incubation to reach significant editing in *L. major* parasites. We previously attempted to minimize these species-specific variations by segregating the CBE expression from the CBE sgRNA cassette in a dual construct system and by employing a T7 RNAP promoter for CBE sgRNA expression (Figure 1B). However, upon transfection of CBE sgRNA expression constructs into *L. major* T7 RNAP- and CBE-expressing parasites, the doubling time increased from 7 to about 14 hours, highlighting a significant growth defect through T7 RNAP-driven CBE sgRNA expression. On the contrary, we observed higher editing rates in a shorter period of time compared to our approach with the single plasmid ribosomal promoter system, indicating potential advantages (Engstler and Beneke, 2023).

Here, our first aim was to eliminate this growth defect observed in the dual construct system while maintaining high editing rates. Assuming that the growth defect resulted from excessive CBE sgRNA expression, we wondered whether modifying the T7 RNAP promoter sequence and altering the transcription initiation site could alleviate the observed toxicity. We therefore introduced a variety of CBE sgRNA expression plasmids into our previously established *L. major* cell line, expressing CBE and T7 RNAP from the β-tubulin locus, as well as tdTomato from the 18S rRNA locus (Engstler and Beneke, 2023) (Figure 1B). To drive CBE sgRNA expression, we thereby utilized two T7 RNAP promoter variants (T7 T-10 and T7 G-10), known for their ability to reduce transcription activity in the closely related parasite *Trypanosoma brucei* (Wirtz et al., 1998). We also manipulated the transcription initiation site by altering the number of guanines (either two or one), a factor believed to impact transcription yield (Padmanabhan et al., 2020) (Figure 1C). Additionally, we compared CBE sgRNA expression via T7 RNAP promoters with the ribosomal promoter derived from *L. donovani*, either in a single or dual construct system setup. For our measurements, we transfected CBE sgRNA expression plasmids with two tdTomato-targeting CBE sgRNAs. While the ‘target’ CBE sgRNA was designed to yield an early STOP codon through C to T conversion, the ‘control’ CBE sgRNA was designed to induce a C to T conversion that results in a neutral substitution (codon change but no amino acid change). Following transfection, we then analysed growth rates (Figure 1D) and tdTomato reporter signals in the resulting non-clonal populations (Figure 1E and F). Our aim was to identify the promoter variant with the highest activity and least toxicity.

As anticipated, when utilizing the ribosomal promoter for CBE sgRNA expression, the dual construct system resulted in a more significant reduction of the tdTomato reporter signal compared to the single plasmid system. The complete knockdown of the tdTomato reporter was also achieved using all T7 RNAP promoter variants with the dual construct system. While there were no detectable differences in these knockdown efficiencies (Figure 1E and F), there were notable variations in the growth rates

130 (Figure 1D). Consistent with our prior observations (Engstler and Beneke, 2023), cells transfected
131 with constructs containing the unmodified T7 RNAP promoter sequence (T7 wt GG in Figure 1D)
132 exhibited an almost two-fold increase in doubling time. On the contrary, employing for CBE sgRNA
133 expression the T7 T10 GG, T7 G10 GG and ribosomal promoter resulted in no significant growth rate
134 increase. The doubling times here ranged from 7.5 to 8.1 hours. While this aligned with
135 measurements obtained for cells transfected with our single plasmid system (Figure 1D), the
136 complete knockdown of the tdTomato reporter was much more rapid using any dual construct system
137 (Figure 1E). Specifically, the complete depletion of the tdTomato reporter signal was achieved in just
138 seven days (Figure 1E) compared to 33 days when using the same CBE sgRNA in *L. major* parasites
139 previously (Engstler and Beneke, 2023). Compared to our first toolkit version (Engstler and Beneke,
140 2023), this demonstrates a major improvement in our method to generate loss-of-function mutants in
141 non-clonal populations.

142 **DSBs introduced by AsCas12a ultra increase integration rates of donor DNA constructs**

143 Having successfully improved editing efficiencies, while at the same time reducing the toxicity of CBE
144 sgRNA expression and targeting, we next attempted to increase transfection rates of the CBE sgRNA
145 expression constructs. Previously, we have shown that ~30,000 *L. mexicana* wildtype cells need to be
146 transfected with our single plasmid system (Figure 1A) to obtain one transfectant (Engstler and
147 Beneke, 2023). Since genomic dropout screens need to be performed at a high representation of
148 about 500 cells per sgRNA construct (Sanjana et al., 2014; Yau and Rana, 2018), this relatively low
149 transfection rate would make any large-scale screen challenging. In addition, we wanted to enable
150 screening of base editor libraries over long periods and in complex environments, such as *in vivo*
151 experiments, without risking that parasites would lose their CBE sgRNA plasmid, vary their plasmid
152 copy number or transfer plasmids between cells. Therefore, we wanted to integrate CBE sgRNA
153 expression constructs into a safe harbor locus. Strategies to increase transfection rates and stably
154 integrate expression cassettes by homologous recombination have been previously developed in
155 *T. brucei*. Here, the use of an I-SceI mega- (Glover and Horn, 2009) or zinc finger- (Schumann et al.,
156 2017) nuclease-induced DSB at a safe harbor locus has been shown to increase the transfection
157 efficiency for the integration of RNAi expression constructs significantly. In combination with improved
158 transfection protocols (Burkard et al., 2007; Glover and Horn, 2009), this has enabled RNAi loss-of-
159 function screens on a genome-wide scale (Glover et al., 2015; Horn, 2022; Schumann Burkard et al.,
160 2011). Alternatively, it has been shown in *Leishmania* that CRISPR/Cas9-induced DSBs can increase
161 the rate of correct donor DNA integration, regardless of homology flank length (Beneke et al., 2017).

162 To develop a strategy for stable integration of CBE sgRNA expression constructs in *Leishmania*
163 species, we decided to employ a Cas12a nuclease variant from *Acidaminococcus* species.
164 Specifically, we generated an expression construct (pTB107 or pTB106) to co-express in *Leishmania*
165 the AsCas12a ultra variant (Zhang et al., 2021), a T7 RNAP and the hyBE4max CBE (Engstler and
166 Beneke, 2023) (Figure 2A). The use of AsCas12a ultra had several advantages compared to other
167 approaches mentioned above. Firstly, compared to the use of I-SceI meganuclease (Glover and Horn,
168 2009), it allowed us to select any TTTV-PAM containing locus of interest to insert our CBE sgRNA

169 expression construct, simply by just changing the Cas12a crRNA sequence. Secondly, Cas12a
170 editing – just like any CRISPR strategy – is much simpler to design than a zinc-finger nuclease
171 (Schumann et al., 2017) or TALENs approach. Thirdly, compared to a functional SpCas9 nuclease,
172 there was no risk of interference between the Cas9 base editor and Cas9 nuclease sgRNAs. Finally,
173 since AsCas12a has an intrinsic RNase activity that allows processing of its own crRNA array (Paul
174 and Montoya, 2020), multiplexing of guide sequences is possible, which could expand the scope of
175 standard CRISPR knockin and knockout approaches in *Leishmania* in future studies. For example,
176 Cas12a crRNA arrays with four or more guides can be assembled and transfected to introduce
177 multiple DSBs within one gene. Since Cas12a generates sticky DNA ends that facilitate
178 recombination via microhomology-mediated end joining and homologous recombination (Zhang et al.,
179 2021), this approach could effectively disrupt target genes without requiring the addition of donor DNA
180 and this may provide an alternative approach to our here presented base editing method in the future.
181 Moreover, CBE sgRNAs could be multiplexed by interspacing them with Cas12a direct repeats (DRs),
182 enabling simultaneous targeting of multiple genes in one cell. Ultimately, we figured that the co-
183 expression of the AsCas12a ultra nuclease, a T7 RNAP and the CBE would generate a hybrid gene
184 editing toolbox that has many possible applications.

185 To introduce AsCas12a-mediated DSBs, we decided to adapt the LeishGEdit approach, which was
186 previously developed for *in vivo* transcription of Cas9 sgRNAs (Beneke and Gluenz, 2019; Beneke et
187 al., 2017). Specifically, we designed two overlapping oligos capable of being mutually amplified,
188 generating a Cas12a crRNA template DNA (Figure 2B). This resulting template featured an
189 unmodified T7 RNAP promoter sequence, facilitating the *in vivo* transcription of the Cas12a crRNA.
190 To ensure high binding affinity of AsCas12a with its Cas12a crRNA, we used an optimized DR from
191 DeWeirdt et al. (2021). Subsequently, this enabled AsCas12a ultra-mediated DSBs for donor DNA
192 integration. To test this approach, we utilized a donor DNA construct containing mNeonGreen (mNG)
193 as a reporter and blasticidin as a resistance marker, allowing for a relatively straightforward
194 assessment of integration accuracy and transfection rate (Figure 2A). Additionally, we varied the
195 length of homology flanks to investigate whether Cas12a-mediated integration of donor DNA
196 remained independent of homology flank length, as previously observed with Cas9 (Beneke et al.,
197 2017). Using homology flanks routinely used for integration into the 18S rRNA safe harbor locus of
198 various *Leishmania* species (Misslitz et al., 2000; Sorensen et al., 2003), we then designed one
199 Cas12a crRNA targeting the 200 bp region between both homology regions (Figure 2 S1A). To
200 evaluate if Cas12a could enhance the transfection rate, we compared transfections of these reporter
201 constructs with and without the addition of Cas12a crRNA.

202 Like findings with Cas9, we observed that Cas12a-induced DSBs in *L. mexicana* increased the rate of
203 correct donor DNA integration, irrespective of homology flank length. Integration of reporter constructs
204 with 600 nt homology flanks showed no difference in reporter signal (Figure 2C), but the addition of
205 Cas12a crRNA boosted transfection efficiency by approximately 25-fold when assessing blasticidin-
206 resistance rates (Figure 2D). When reducing homology flank length to 60 nt, we observed no impact
207 on the reporter signal or transfection rate when Cas12a crRNA was present during transfections.

208 However, in the absence of Cas12a crRNA, no transfectants were obtained, confirming that
209 homologous recombination of the reporter is only independent of homology flank length if a Cas12a-
210 mediated DSB has occurred. Further reducing the homology flank length to 30 nt did not significantly
211 decrease transfection efficiency. However, the percentage of mNG positive cells decreased from
212 ~99% in all other samples to 96.7% (Figure 2C), likely due to imprecise recombination events in some
213 cells. Conversely, Sanger sequencing the integration sites of these non-clonal populations indicated
214 flawless recombination for all constructs (Figure 2 S1A, B and C). Interestingly, diversity in the
215 reporter signal was also noted when transfecting the mNG construct as an episome (Figure 2C),
216 possibly pointing towards plasmid copy number variants between transfected cells. In addition,
217 episomal transfections using the same number of DNA molecules resulted in a significantly lower
218 number of transfectants (Figure 2D), concluding the advantages of integrating expression constructs
219 via Cas12a-mediated DSBs.

220 We then wondered whether employing different Cas12a crRNAs could enhance the transfection
221 efficiency even further. Three additional Cas12a crRNAs within the 18S rRNA SSU locus were
222 selected for testing (Figure 2 S1D). In addition, we sought to examine the integration into a "landing-
223 pad", such as a previously introduced resistance marker. We expected that this would further increase
224 the accuracy and efficiency of the transfection. We therefore decided to test our system in a
225 tdTomato-expressing *L. mexicana* cell line (Engstler and Beneke, 2023) and designed two Cas12a
226 crRNAs to integrate mNG-blasticidin donor DNA constructs within their neomycin-resistance marker
227 (Figure 2 S1D). Given that 60 nt homology flank length was sufficient for accurate and efficient
228 integration of donor DNA (Figure 2C and D), we decided to test all six Cas12a crRNAs in combination
229 with donor DNA constructs containing 60nt homology flanks. This meant that homology flanks could
230 be easily adapted through long-primer PCR without the need for bacterial cloning.

231 Across all six Cas12a crRNAs tested, no significant changes in the proportion of mNG-expressing
232 cells were observed when analyzing non-clonal populations post-transfection (Figure 2E). However,
233 there was a substantial variation in the rate of blasticidin-resistant cells, indicative of Cas12a crRNA
234 efficiency (Figure 2F). For Cas12a crRNA-1, we confirmed our previous results, yielding one
235 transfectant per ~8,500 transfected cells. However, other Cas12a crRNAs, particularly Cas12a
236 crRNA-4, performed significantly better, resulting in one transfectant out of approximately 2,300
237 transfected cells. Interestingly, despite being only 44bp upstream of Cas12a crRNA-4, Cas12a
238 crRNA-3 exhibited a 500-fold lower integration efficiency. Surprisingly, both neomycin-targeting
239 Cas12a crRNAs were less efficient than the majority of 18S rRNA SSU locus-targeting guides (Figure
240 2F). Given the exceptional efficiency of Cas12a crRNA-4, we verified the integration of donor DNA at
241 its site in the non-clonal population through Sanger sequencing, confirming flawless integration
242 (Figure 2 S1D, E, and F).

243 **Integration of CBE sgRNA expression cassettes via AsCas12a ultra-introduced DSBs increase**
244 **editing rates**

245 After successfully validating our here developed AsCas12a ultra-mediated integration system, we
246 then decided to combine our Cas12a knock-in system with our optimized CBE sgRNA expression

247 cassette (Figure 3A). For this purpose, we developed two CBE sgRNA expression plasmids, namely
248 pTB104 and pTB105, each incorporating a puromycin-resistance marker and the most effective T7
249 RNAP promoter variant (T7 T10 GG) for CBE sgRNA expression (as identified in assays above;
250 Figure 1C, D and E). While pTB104 featured 350 nt homology flanks adjacent to the neomycin-
251 targeting Cas12a crRNA-6, pTB105 included 350 nt homology flanks adjacent to our best-performing
252 Cas12a crRNA-4, targeting the 18S rRNA SSU locus. This design allowed for the integration of both
253 CBE sgRNA expression cassettes with and without the addition of Cas12a crRNAs. To assess if such
254 a system could effectively generate a functional null mutant through cytosine-to-thymine conversion,
255 we chose to target tdTomato again and tested a tdTomato-targeting CBE sgRNA in *L. donovani*,
256 *L. mexicana*, and *L. major*. Parasites expressed tdTomato, along with the CBE, Cas12a ultra, and T7
257 RNAP (Figure 3A). Additionally, we investigated whether the efficiency of the tdTomato knockdown
258 would be influenced by how the CBE sgRNA expression cassette was integrated. We therefore
259 compared Cas12a crRNA-4 and 6 in combination with 60 and 350 nt homology flanks.

260 Strikingly, we observed a complete depletion of the tdTomato signal just 7 days post transfection in all
261 tested species when integrating CBE sgRNA expression cassettes into the 18S rRNA SSU locus.
262 This occurred irrespective of homology flank length. However, integrating cassettes into the neomycin
263 resistance marker ("landing-pad approach") resulted in only partial tdTomato knockdowns in *L. major*
264 and *L. donovani*, while a complete knockdown could again be achieved in *L. mexicana*. Although we
265 have not further investigated the cause for this, we assume that either the low efficiency of Cas12a
266 crRNA-6 or the number of tdTomato-neomycin-expression cassettes caused this discrepancy. Overall,
267 this highlights that integrating CBE sgRNA expression cassettes into the 18S rRNA SSU locus using
268 Cas12a crRNA-4 in combination with plasmid pTB105 would yield the highest CBE sgRNA editing
269 efficiency. We therefore tested next the transfection rate of CBE sgRNA expression cassettes using
270 Cas12a crRNA-4 for integration in *L. mexicana*, *L. major* and *L. donovani*. We reached high
271 transfection efficiencies, yielding up to one transfectant out of ~470 transfected *Leishmania* parasites,
272 with *L. donovani* being the most and *L. major* being the least efficient (Figure 3C, left panel).

273 We then wondered whether we could increase the transfection efficiency even further by using the
274 Lonza Nucleofector technology. Previous studies in *T. brucei* demonstrated that the improved
275 transfection rate achieved through I-SceI meganuclease-mediated cleavage could be further
276 increased when combined with the Lonza Nucleofector technology, resulting in up to one transfectant
277 per 100 transfected cells (Glover and Horn, 2009). Considering this, we explored whether this
278 approach would be as effective in *Leishmania* parasites. We therefore conducted a side-by-side
279 comparison of the transfection efficiency between the Lonza Nucleofector Basic Parasite kit and the
280 *Trypanosoma*-optimized buffer (Tb-BSF buffer, see method section for further details) (Schumann
281 Burkard et al., 2011), both in combination with an Amaxa Nucleofector 2b electroporator. To increase
282 the number of parasites per transfection even further, we compared our standard transfection protocol
283 using 5×10^6 cells per transfection with up-scaled transfection formats involving 1×10^8 cells and
284 2.5×10^8 cells per electroporation. Testing these conditions in *L. mexicana*, we confirmed that the
285 Lonza Nucleofector technology could indeed boost transfection efficiency by an additional 20-fold

286 (Figure 3C, right panel). When transfecting 1×10^8 cells per transfection with 10 µg of PacI-linearized
287 pTB105 plasmid DNA, we achieved up to one transfectant out of 70 transfected cells (Figure 3C, right
288 panel). This represents a more than 400-fold increase in transfection efficiency compared to our
289 previous rates (Engstler and Beneke, 2023). Moreover, it demonstrates that a CBE sgRNA library with
290 40,000 constructs could be transfected at a representation rate of 500-fold using just 20×10^8 cells
291 across 20 transfection cuvettes. Ensuring a 500-fold library representation represents a substantial
292 improvement compared to previous RNAi screens in *T. brucei*, where screens typically achieved
293 about 5-9-fold library representation (Glover et al., 2015; Horn, 2022; Morris et al., 2002; Schumann
294 Burkard et al., 2011). This high representation rate is considered crucial for large-scale dropout
295 screens, as it can affect hit identification by minimizing variations between replicates. However, it's
296 worth noting that drug resistance screens can also be conducted at much lower coverage (Sanjana et
297 al., 2014; Yau and Rana, 2018).

298 While the significantly enhanced transfection rates are a central aspect of our improved base editing
299 method presented here, it is crucial to emphasize that these improvements were achieved without
300 impacting parasite growth. Through an assessment of doubling times in transfected and parental cell
301 lines, we confirmed that the expression of CBE, T7 RNAP, AsCas12a ultra, and the CBE sgRNA had
302 minimal or no impact on parasite growth across all three species (Figure 3D). This marks a substantial
303 improvement, considering that the expression of CBE and/or CBE sgRNA in our first toolbox version,
304 using the pLdCH-hyBEmax plasmid, could lead to significant growth defects in some *Leishmania*
305 species (Engstler and Beneke, 2023).

306 Having established this optimised system, we next decided to target PF16, a gene encoding a central
307 pair protein of the axoneme that has been demonstrated to be essential for *Leishmania* flagellar
308 motility (Beneke et al., 2017; Engstler and Beneke, 2023; Martel et al., 2017). For our test, we chose
309 to utilize a previously employed PF16-targeting CBE sgRNA, namely PF16-3. This specific CBE
310 sgRNA induces paralysis in *Leishmania* parasites by introducing a thymidine homo-polymer ("TTTTT")
311 within the PF16 coding sequence. While our usual design for CBE sgRNAs aims to introduce STOP
312 codons through cytosine-to-thymine conversion, we selected PF16-3 for this test because its editing
313 activities are known to vary across species (Engstler and Beneke, 2023). In earlier attempts, we had
314 to express CBE sgRNA PF16-3 in non-clonal populations for 42 days to achieve sufficient editing in
315 *L. major* when using our pLdCH-hyBE4max single vector (Figure 1A) (Engstler and Beneke, 2023).
316 Meanwhile, in *L. donovani*, high editing rates were already achieved 14 days post transfection. Now,
317 we expected that editing rates had improved uniformly across all species.

318 As anticipated, we observed a significant increase in editing activity in *L. major* parasites. Just 14
319 days post transfection, we found that the homo-polymer had been fully introduced in non-clonal
320 populations when using our T7 RNAP promoter-based dual vector system, while no editing could be
321 observed using the ribosomal promoter single vector system at this time point (Figure 4B, *L. major*
322 panel). This was also reflected in the analysis of mutant swimming speed, revealing clear motility
323 defects in respective transfectants (Figure 4A, *L. major* panel).

324 We next proceeded to test our optimized system also in *L. mexicana* and *L. donovani* parasites, once
325 again employing Cas12a for integration of the CBE sgRNA expression construct. However, here we
326 chose to target PF16 in two cell lines: (i) one that possessed the pTB107 construct and a tdTomato
327 reporter, and (ii) one that possessed the pTB107 construct only (WT pTB107). Additionally, we took
328 this opportunity to compare motility and CBE editing rates in cells that had been transfected with
329 Cas12a crRNAs that target the neomycin-resistance marker (Cas12a crRNA-6) and the 18S rRNA
330 SSU locus (Cas12a crRNA-4).

331 Our results clearly showed that just 6 days post transfection, the PF16 target site was fully edited, and
332 the overwhelming majority of all cells were paralyzed in all tested scenarios (Figure 4A and B).
333 However, surprisingly editing slowly reversed in *L. mexicana* cells harboring the pTB107 construct
334 only (Figure 4A and B). Although we decided not to further investigate the reason for this unexpected
335 result, we assumed that it might be caused by a small proportion of cells where the CBE sgRNA
336 expression cassette was incorrectly integrated. This could potentially result in the silencing of the CBE
337 sgRNA expression or even lead to the deletion of the guide cassette. Since the PF16 mutation in
338 *L. mexicana* is known to be associated with a mild growth defect (Beneke et al., 2019), PF16-deficient
339 mutants would eventually be outcompeted over time, leading slowly to the reversal of editing rates.
340 While this escape or reversal of mutant phenotypes might initially appear problematic for detecting
341 growth-associated or other phenotypes in pooled screens, it is important to note that this
342 phenomenon has also been observed with other loss-of-function tools. For instance, RNAi escape
343 has been reported in *T. brucei* when targeting growth-associated genes (Ariyanayagam et al., 2005;
344 Schlecker et al., 2005). Nevertheless, genome-wide loss-of-function screens have been successfully
345 performed in these parasites (Alsford et al., 2011). But more importantly the reversal of the PF16
346 mutation was not observed in any other tested cell line when comparing editing and motility rates 6
347 and 16 days post transfection. Both tested *L. donovani* cell lines and the tested *L. mexicana* cell line
348 that possessed the pTB107 construct and the tdTomato expression cassette (Figure 4A and B)
349 remained paralyzed over the entire observation time. To confirm that these cells would have no
350 potential ever to reverse their phenotype, we decided to Illumina sequence these non-clonal
351 paralyzed *L. mexicana* PF16 mutant populations 16 days post transfection. Analyzing their
352 sequencing data, we did not find a single read of an unedited PF16 CDS sequence (with
353 approximately 35× genome coverage), confirming that indeed all cells within this transfected non-
354 clonal population were completely mutated (Figure 4 S1A).

355 **Cas12a-mediated DSB ensures the integration of one CBE sgRNA per *L. mexicana* transfectant**

356 We next wanted to verify how exactly the CBE sgRNA expression cassette had been integrated via
357 Cas12a-mediated DSB in these non-clonal *L. mexicana* populations that possessed the pTB107
358 construct and the tdTomato reporter, as well as the PF16-targeting CBE sgRNA expression construct
359 16 days post transfection. Since the tdTomato expression cassette is just ~400 nt upstream of the
360 Cas12a crRNA-4 target sequence, we wondered whether it had come to any obvious interference
361 between the tdTomato and CBE sgRNA expression cassettes. Given the highly repetitive nature of
362 the 18S rRNA SSU locus, we employed Oxford Nanopore Technology (ONT) sequencing to

363 determine the exact integration pattern of both cassettes. For the analysis of sequencing reads, we
364 mapped them against two customized genomes. In the first genome, we assumed that the tdTomato
365 expression cassette was integrated separately from the CBE sgRNA construct, implying that each
366 cassette had integrated on the opposite allele (Figure 4 S1B). In the second genome, we assumed
367 that both cassettes were integrated on the same allele and could be detected on a single ONT read
368 (Figure 4 S1C).

369 Interestingly, we could only map unique ONT reads to the first scenario, where cassettes were
370 assumed to be integrated on separate alleles and present in only one copy in the genome. These
371 ONT reads covered the entire tdTomato or CBE sgRNA expression cassette, as well as sequences
372 adjacent to homology flanks used for integration (Figure 4 S1B and C).

373 We also used our ONT data to validate whether the tdTomato and CBE sgRNA expression cassettes
374 (Figure 4 S2A) had integrated into any unintended genetic loci. The coding sequence of the tdTomato
375 reporter gene and the sgRNA expression cassette, comprising the optimized T7 RNAP promoter (T7
376 T10 GG), PF16-3 targeting spacer, and Cas9 sgRNA scaffold sequence, were analysed using a
377 standard nucleotide BLAST search (Figure 4 S2B). Then, all matched ONT reads were extracted and
378 we verified whether the full expression cassettes (Figure 4 S2A) were correctly integrated at the
379 intended position within the 18S rRNA SSU locus. As expected, all identified cassettes in the
380 extracted contigs were correctly integrated (Figure 4 S2C and D). Importantly, no ONT reads
381 containing the tdTomato or CBE sgRNA cassettes could be linked to any other locus. Moreover, no
382 contigs contained multiple or both, the tdTomato and CBE sgRNA expression cassettes, suggesting
383 again that these cassettes had integrated into opposite alleles and are present in only one copy in the
384 genome.

385 To validate our findings, we then revisited our Illumina sequencing data and analysed the coverage of
386 relevant genetic features. Specifically, we normalized all reads to the total number of reads per
387 chromosome and compared the normalized coverage of reads mapped to the CDS of PF16, the CBE
388 sgRNA cassette, the CDS of tdTomato, and the CDS of the neomycin-resistance marker. While we
389 found equal read coverage of PF16-mapped reads and the chromosome harboring PF16, read
390 coverage for the CBE sgRNA cassette, the CDS of tdTomato, and the CDS of the neomycin-
391 resistance marker were approximately half of the read coverage of their harboring chromosome 27
392 (Figure 4 S1D). This further confirmed our hypothesis that indeed the CBE sgRNA expression
393 cassette had only been integrated on one allele, and most likely, this meant that only one CBE sgRNA
394 cassette copy was present per *L. mexicana* cell. Given that the recognition site of Cas12a crRNA-4 is
395 contained within the homology flank used for tdTomato integration at the 18S rRNA locus, this may
396 contribute to the integration pattern we observe. But since the homology sequences are identical to
397 the original sequences at the locus, the reasons to why this affects the integration of the CBE sgRNA
398 expression cassettes remain unclear.

399 Nevertheless this represents an improvement since, in our previously used single vector episomal
400 system, approximately one-third of all *L. mexicana* transfectants possessed more than one CBE-

401 sgRNA expression plasmid, potentially causing combinatorial knockout effects (Engstler and Beneke,
402 2023). To verify that in our new dual system each cell indeed harboured only one CBE sgRNA, we
403 decided to test if isolated clones from a transfected library would possess one or multiple CBE sgRNA
404 sequences. In addition to testing this in *L. mexicana*, we also wanted to assess this for *L. donovani*
405 *and L. major*, as we had not sequenced respective mutants via ONT and Illumina sequencing.

406 Using again Cas12a crRNA-4 for the integration of a small-scale pTB105 CBE sgRNA expression
407 cassette library (containing 13 different CBE sgRNA sequences), we isolated 10 clones from each
408 species, PCR amplified the integrated CBE sgRNA locus, and sequenced it by Sanger sequencing.
409 As expected, we found only unique sequencing reads for all tested *L. mexicana* clones, confirming the
410 integration of only one guide per transfectant (Figure 4 S3). However, for *L. donovani* and *L. major*, 2
411 out of 10 sequencing reads showed mixed guide sequences (Figure 4 S3), suggesting that multiple
412 CBE sgRNAs can be integrated per cell. Furthermore, the integration of multiple sgRNAs per cell
413 remained random. While testing other Cas12a crRNAs in the future may identify a more unique
414 integration locus for *L. donovani* and *L. major* parasites, any compensatory effects through the
415 integration of multiple CBE sgRNAs in these species will likely be minimal and presumably not
416 detectable in large-scale screens with a high library representation rate. Alternatively, a "landing pad"
417 for integrating CBE sgRNA expression cassettes could be used, such as the neomycin resistance
418 gene targeted by the Cas12a crRNA-6 presented here (Figure 2F, 2S1D, and 4). Therefore, we
419 believe that this method is suitable not only for screens in *L. mexicana* but also in *L. donovani* and
420 *L. major*.

421 **Detection of fitness-associated phenotypes in a pooled loss-of-function screen**

422 To provide evidence that our improved CRISPR base editing system can indeed detect a range of
423 mutant phenotypes in pooled screens, including fitness-associated phenotypes, and to confirm
424 significant improvements over our previous method (Engstler and Beneke, 2023), we next performed
425 a small-scale loss-of-function fitness screen in *L. mexicana* parasites. First, we pooled 39 CBE
426 sgRNAs and cloned them into pTB105, the vector designed for integration into the 18S rRNA locus
427 using the best-performing Cas12a guide, crRNA-4. Of these sgRNAs, 24 were designed to introduce
428 a STOP codon within the first half of ORFs essential for survival or normal proliferation in
429 promastigote culture. Targeted genes included five essential kinases for which null mutants could not
430 be generated in individual studies or in the kinome-wide bar-seq screen carried out by Baker and
431 colleagues (Baker et al., 2021). These included casein kinase 1 isoform 2 (CK1.2) (Rachidi et al.,
432 2014), cdc2-related kinase 2 and 3 (CRK2, CRK3) (Duncan et al., 2016; Hassan et al., 2001;
433 Yagoubat et al., 2020), Aurora kinase 1 (AUK1/AIRK) (Chhajer et al., 2016) and target of rapamycin
434 kinase (TOR) 1 (Madeira da Silva and Beverley, 2010). We also included sgRNAs targeting the Ras-
435 related protein (Rab) 5a, believed to be essential as null mutants could not be generated (Rastogi et
436 al., 2016), and sgRNAs targeting three intraflagellar transport (IFT) proteins (IFT139, IFT140, and
437 IFT88), all predicted to result in growth associated phenotypes (Beneke et al., 2019; Beneke et al.,
438 2024; Sunter et al., 2018). As a control, our library included also 15 non-targeting sgRNA with random
439 sequences (Doench et al., 2016).

440 The PacI-linearized library was then co-transfected with Cas12a crRNA-4 template DNA into
441 *L. mexicana* carrying the pTB107 construct and the tdTomato expression cassette (Figure 5A). As
442 shown earlier (Figure 4), these parasites did not reverse their phenotype when inducing a PF16
443 mutation. A second cell line with an alternative pTB107 construct, pTB106, containing the
444 *Leishmania*-derived Rad51 single-stranded DNA-binding domain - previously shown to enhance
445 cytosine base editing rates (Engstler and Beneke, 2023) - was also used (Figure 5A). Following
446 transfection in three independent replicates, cells were selected for CBE sgRNA library integration at
447 the 18S rRNA locus and cultured for 288 hours before undergoing Illumina amplicon sequencing
448 (Figure 5B and C). The data analysis compared sgRNA ratios before and after transfection at various
449 time points (Figure 5D). As expected, sgRNAs targeting essential and fitness-associated genes were
450 strongly depleted, in contrast to non-targeting control sgRNAs, which remained unchanged. Notably,
451 only two IFT88, two CRK3, and one CRK2 sgRNAs showed no reduction in abundance, while all
452 other sgRNAs moved significantly outside the 99% confidence interval of the non-targeting controls
453 (Figure 5D). With a representation rate of ~25,000 cells/sgRNA, triplicate error margins were small.
454 However, no substantial differences were observed between the two Rad51 variants used in the CBE
455 system (Figure 5D). Lastly, we compared the data from our improved base editing method with results
456 from a previous screen conducted using our first base editing method version (Engstler and Beneke,
457 2023). The comparison between method v1 and v2 revealed significant improvements: for one sgRNA
458 targeting IFT88 and another targeting CRK3, the new method achieved ~10-20x stronger ratios with
459 substantially reduced error margins for the non-targeting controls, enabling more accurate
460 classification of fitness-associated genes (Figure 5E). Overall, these results demonstrate that our
461 method has been significantly improved, enabling robust and scalable loss-of-function screens to
462 identify essential and fitness-associated genes in the future. Notably, we have now completed the first
463 genome-wide functional screens in *Leishmania* species using libraries containing up to 40,000
464 sgRNAs (Beneke lab, manuscript in preparation).

465 **Improved CBE sgRNA design to prioritize edits resulting only in STOP codons**

466 The results above demonstrate that Cas12a crRNAs can be used to efficiently integrate CBE sgRNA
467 expression cassettes and libraries into *Leishmania* species. This has no significant impact on parasite
468 growth and enables high editing rates in all these tested species. The utility of fitness screens is also
469 demonstrated. However, as we noted in our previous study (Engstler and Beneke, 2023), high editing
470 rates do not necessarily lead to a strong knockdown of the targeted protein. Cells with a deleterious
471 mutation can be simply outcompeted by cells with a non-deleterious mutation. This issue is
472 particularly relevant when not all available cytosine nucleotides within the CBE sgRNA editing window
473 result in a STOP codon after thymine conversion. To address this, we have therefore improved the
474 scoring of previously designed CBE sgRNAs by implementing a C-score that determines the ratio of
475 available cytosines to resulting STOP codons (Figure 4 S4). This new scoring system has been
476 uploaded to www.leishbaseedit.net and will be systematically tested in future studies, e.g. by using
477 editing reporters. We also considered the position at which the STOP codon would occur and
478 designed a scoring matrix that rates CBE sgRNAs higher when the STOP codon is introduced within
479 positions 4-8 and lower when introduced within positions 11-12 (Figure 4 S4). While our ratio scoring

480 aims to increase the chance of successfully generating a functional mutation through STOP codon
481 insertion, it is important to note that the introduction of a STOP codon is not the only efficient way to
482 generate a functional mutant. As shown above, the introduction of a thymidine homo-polymer
483 ("TTTTT") within the PF16 CDS produces the same motility phenotype observed when using gene
484 replacement strategies for knockout generation (Beneke et al., 2017). Ultimately, this expands the
485 possibilities for upcoming mutational screens in *Leishmania*.

486 **Co-expression of Cas12a and CBE enables a wide range of genetic manipulations**

487 While these modifications to our sgRNA scoring tool represent a hypothetical but yet promising
488 improvement in our method, the design of our triple expression construct (AsCas12a ultra, T7 RNAP,
489 and Cas9 CBE) also offers opportunities for other advancements. For example, it enables hybrid
490 approaches where classical CRISPR gene replacement and/or tagging methods can be combined
491 with cytosine base editing experiments in one cell line. This is particularly interesting for targeting
492 multiple genes simultaneously or dispersed multi-copy genes, and can also include the co-targeting of
493 non-coding and coding genetic elements. Furthermore, since Cas12a has an intrinsic RNA cleavage
494 activity, multiplexing of sgRNAs is possible and this expands the range of potential applications
495 further as outlined above.

496 To explore the applicability of AsCas12a ultra for gene replacement strategies, such as the
497 LeishGEdit approach (Beneke and Gluenz, 2019; Beneke and Gluenz, 2020; Beneke et al., 2017), we
498 devised two Cas12a crRNAs targeting the 5' and 3' UTR of the PF16 ORF (Figure 6A). Additionally,
499 we designed 30nt homology flanks adjacent to these crRNAs. We then PCR-amplified pTBlast and
500 pTPuro cassettes from the LeishGEdit toolbox using primers containing these homology flanks and
501 co-transfected them with Cas12a crRNA template DNA into *L. mexicana* parasites. These cells
502 contained the pTB107 construct for co-expression of AsCas12a ultra, T7 RNAP, and CBE. Like the
503 Cas9 LeishGEdit approach, transfected Cas12a crRNAs contained a T7 RNAP promoter for efficient
504 *in vivo* transcription (Figure 2B). Following transfection, we then confirmed that the ORF was
505 successfully replaced by drug resistance markers on both alleles and amplified the PF16 locus with
506 two ORF spanning primers (Figure 6A and B). In addition, we performed Sanger sequencing over
507 integration flanks to verify the integration of donor DNA fragments. This analysis confirmed the
508 accurate integration of both donor DNA constructs (Figure 6C and D). Lastly, we performed again our
509 motility analysis on these mutants, revealing the expected PF16 motility phenotype (Figure 6E).
510 Overall, this demonstrates the versatility of our AsCas12a ultra, T7 RNAP, and CBE co-expression
511 vector for a wide range of CRISPR applications in *Leishmania*.

512 **Conclusion**

513 The *Leishmania* research community faces significant challenges in systematically assessing the
514 function of all genes within the species. The absence of a functional NHEJ pathway complicates the
515 process of obtaining null mutants, typically demanding the additional use of donor DNA, selection of
516 edits associated with drug resistance, or the time-consuming isolation of clones. These complexities
517 also apply to loss-of-function screens. While pooled CRISPR screens that rely solely on sgRNA
518 expression are feasible to some extend for drug-resistance studies in *Leishmania* (Queffeulou et al.,

519 2024), they are less likely to succeed in fitness-related phenotypic screens. While, bar-seq screens
520 (Baker et al., 2021; Beneke et al., 2019; Beneke and Gluenz, 2020) and RNAi methods (de Paiva et
521 al., 2015; Lye et al., 2022) offer potential solutions, they come with clear limitations. Most notably, the
522 use of RNAi is restricted to *Leishmania* species within the *Viannia* subgenus, and bar-seq screens
523 pose logistical challenges due to the necessity of generating thousands of individually created
524 mutants. Furthermore, CRISPR gene replacement approaches, such as bar-seq methods, require
525 multiple rounds of transfection when targeting dispersed multi-copy genes and are not suited to
526 mutate interrupted tandemly arrayed coding and non-coding genes, which are abundantly present in
527 the *Leishmania* genome.

528 Therefore, we recently introduced cytosine base editing as an alternative method for gene editing and
529 large-scale screening in *Leishmania*, aiming to overcome these limitations. However, variations in
530 editing efficiency, substantial reduction in parasite growth, competition between deleterious and non-
531 deleterious mutations, and low transfection rates prompted further refinements of our method. Here
532 we present major improvements that collectively enhance our CBE method for *Leishmania* parasites.

533 In our final setup, we effectively employ a dual construct system, where a stable cell line is
534 transfected with a CBE sgRNA expression construct. The stable cell line expresses the hyBE4max
535 CBE, AsCas12a ultra, and T7 RNAP, with CBE sgRNA expression driven by a T7 RNAP promoter
536 variant (T7 T-10 GG). Alongside our updated CBE sgRNA design tool, which now prioritizes sgRNAs
537 with a low cytosine to resulting STOP codon ratio, this system achieves high editing rates without
538 affecting parasite growth. Compared to our initial CBE single-vector method, this dual-construct
539 system has the disadvantage that it requires the generation of a stable cell line first. However, it offers
540 the clear advantage that CBE sgRNA expression constructs can be efficiently integrated using
541 AsCas12a-mediated DSBs. Through testing a series of Cas12a crRNAs, we identified a specific
542 Cas12a crRNA capable of efficiently integrating CBE sgRNA expression cassettes into the 18S rRNA
543 SSU safe harbor locus. CBE sgRNA expression cassettes can thereby be generated by amplification
544 or digestion of the plasmid pTB105. In combination with the Lonza Nucleofector technology, this
545 approach increases transfection rates by ~400-fold, yielding up to 1 transfectant per 70 transfected
546 cells. This improved base editing method enabled the successful execution of a small-scale loss-of-
547 function screen, confirming the essential and/or growth-associated roles of several kinases (CK1.2,
548 CRK2, CRK3, AUK1/AIRK, and TOR1), as well as proteins related to intraflagellar transport (IFT88,
549 IFT139, and IFT140) and endocytosis (Rab5A). Lastly, the co-expression of Cas12a and CBE
550 provides strategic advantages, enabling the use of CRISPR gene replacement and base editing
551 approaches in the same cell line. Moreover, Cas12a can be easily employed for protein tagging and
552 multiplexing of sgRNAs, offering in the future a wide range of possible editing experiments in
553 combination with base editing. Overall, our improved toolbox sets the stage for various gene editing
554 applications in *Leishmania*, including genome-wide cytosine base editor screens, and we believe that
555 these will make significant advancements in the field.

556

557 **MATERIAL AND METHODS**

Key Resources Table				
Reagent type (species) or resource	**Designation**	**Source or reference**	**Identifiers**	**Additional information**
Cell line (*Leishmania mexicana*)	*L. mexicana* wildtype	Eva Gluenz laboratory	WHO strain MNYC/BZ/62/M379	Used TriTrypDB (release 59, (Aslett et al., 2010)) reference annotation: *L. mexicana* MHOMGT2001U1103
Cell line (*Leishmania major*)	*L. major* wildtype	Eva Gluenz laboratory	strain Friedlin	Used TriTrypDB (release 59, (Aslett et al., 2010)) reference annotation: *L. major* Friedlin
Cell line (*Leishmania donovani*)	*L. donovani* wildtype	Joachim Clos laboratory (Decuypere et al., 2005)	strain BPK190	Used TriTrypDB (release 59, (Aslett et al., 2010)) reference annotation: *L. donovani* BPK282A1
Recombinant DNA reagent	pTB007-hyBE4max	(Engstler and Beneke, 2023)		Contains CBE hyBE4max and T7 RNAP
Recombinant DNA reagent	pLdCH-hyBE4max	(Engstler and Beneke, 2023)		Contains CBE hyBE4max and CBE sgRNA
Recombinant DNA reagent	pLdCH-hyBE4max-LmajDBD	(Engstler and Beneke, 2023)		Contains Leishmania-optimised CBE hyBE4max and CBE sgRNA
Recombinant DNA reagent	pTB107	This study		Contains CBE hyBE4max, AsCas12a ultra and T7 RNAP (available in versions with either a hygromycin or phleomycin resistance marker)
Recombinant DNA reagent	pTB106	This study		Contains Leishmania-optimised CBE hyBE4max, AsCas12a ultra and T7 RNAP (available in versions with either a hygromycin or phleomycin resistance marker)
Recombinant DNA reagent	pTB102	This study		Contains T7 RNAP promoter-driven CBE sgRNA expression cassette without homology flanks

Recombinant DNA reagent	pTB104	This study		Contains T7 RNAP promoter-driven CBE sgRNA expression cassette with homology flanks for neomycin-resistance gene
Recombinant DNA reagent	pTB105	This study		Contains T7 RNAP promoter-driven CBE sgRNA expression cassette with homology flanks for 18S rRNA SSU locus
Software	TriTrypDB (release 59)	(Aslett et al., 2010)	https://tritrypdb.org/tritrypdb/app	
Software	LeishBASEedit	This study	http://www.leishbaseedit.net/	See description under "Automated CBE guide design using LeishBASEedit"
Gene (*L. donovani* BPK282A1, *L. major* Friedlin, *L. mexicana* MHOMGT2001U1103)	PF16	TriTrypDB (release 59) (Aslett et al., 2010)	LdBPK_201450.1, LmjF.20.1400, LmxM.20.1400	

558

559 **Cell culture**

560 As described in Engstler and Beneke (2023), promastigote-form *L. mexicana* (WHO strain
561 MNYC/BZ/62/M379), *L. major* Friedlin and *L. donovani* (strain BPK190, (Decuypere et al., 2005))
562 were grown at 28°C in M199 medium (Life Technologies) supplemented with 2.2 g/L NaHCO3,
563 0.0025% haemin, 0.1 mM adenine hemisulfate, 1.2 µg/mL 6-biopterin, 40 mM 4-(2-
564 Hydroxyethyl)piperazine-1-ethanesulfonic acid (HEPES) pH 7.4 and 20% FCS. Media were
565 supplemented with the relevant selection drugs: 40 µg/ml Hygromycin B, 40 µg/ml Puromycin
566 Dihydrochloride and 40 µg/ml G-418 Disulfate. The identity of each *Leishmania* species and absence
567 of mycoplasma contamination was confirmed previously (Engstler and Beneke, 2023). Doubling times
568 were determined as described in Engstler and Beneke (2023).

569 **Cas12a and CBE sgRNA design**

570 For optimizing the CBE targeting of tdTomato and PF16, we selected sgRNAs from Engstler and
571 Beneke (2023) (Supplementary File 1).

572 Cas12a crRNAs were designed using CCTop (Labuhn et al., 2018; Stemmer et al., 2015) with the
573 "PAM type" setting "TTTN" and species specification "Protists – Euglenozoa – *Leishmania tarentolae*".
574 For the Cas12a crRNA sequence search, we selected the 18S rRNA locus from *L. mexicana* (using
575 an ONT-Illumina sequencing optimised MHOMGT2001U1103 genome annotation from Beneke et al.
576 (2022)) and selected homology flanks routinely used for integration into this locus (Misslitz et al., 2000;
577 Sorensen et al., 2003). For designing Cas12a crRNAs that would target a potential "landing-pad", we
578 searched the neomycin-resistance marker for possible spacer sequences. All resulting Cas12a
579 crRNAs were then checked for possible off-targets by using a local blast search against all
580 *Leishmania* species currently available on TritrypDB (release 59, (Aslett et al., 2010)). This ensures
581 that Cas12a crRNAs can be used for specific donor DNA integration in these species.

582 **Plasmid construction**

583 All generated plasmids were subjected to whole plasmid sequencing at Plasmidsaurus and critical
584 sites were additionally subject to Sanger sequencing.

585 Primers were ordered as standard desalted oligos at 25 nmole scale (Sigma). All oligo sequences can
586 be found in Supplementary File 1. Plasmid maps are contained within Supplementary File 2 and can
587 also be downloaded from www.leishbaseedit.net.

588 **Construction of CBE, Cas12a and T7 RNAP co-expression plasmids**

589 We synthesized the open-reading frame (ORF) of AsCas12a ultra (M537R/F870L mutation) (Zhang et
590 al., 2021) with a fused SV40 nuclear localisation signal (NLS), a 3xFLAG tag, a P2A self-cleaving
591 peptide and a c-myc NLS, consisting of six repeats. This c-myc NLS repeat has been previously
592 shown to increase editing activity (Gier et al., 2020). We then amplified the synthesized Cas12a
593 construct in a fusion PCR, adding parts of the T7 RNAP (ORF) and an intergenic region to the

594 construct (using primer-pair 2051F/2052R and 2053F/2054R for amplification from pTB007-
595 hyBE4max). Subsequently, this enabled cloning of the AsCas12a-expression cassette into pTB007-
596 hyBE4max using FseI and AflII. We termed the resulting plasmid pTB107, which allows for the co-
597 expression of AsCas12a ultra, T7 RNAP, hyBE4max CBE and hygromycin resistance-marker. To
598 create a version of pTB107 that contained our previously pioneered *Leishmania*-derived version of the
599 Rad51 single-stranded DNA-binding domain (ssDNA-DBD), we digested pLdCH-hyBE4max-LmajDBD
600 (Engstler and Beneke, 2023) and pTB107 with AvrII and FseI to generate pTB106.

601 **Optimisation of sgRNA expression promoters and construction of sgRNA expression plasmids**
602 **and libraries**

603 For generation of T7 RNAP promoter-driven CBE sgRNA expression plasmids, we amplified and
604 cloned the sgRNA-expression cassette from pLdCH into NsiI and MluI sites of a pPLOT-Puro plasmid
605 (Beneke et al., 2017), thereby introducing the unmodified T7 RNAP promoter sequence (amplification
606 using primer-pair 2128F-WT/2129R). To enable sgRNA cloning using BbsI sites, we then eliminated
607 the BbsI site contained within the Actin 5'UTR of this plasmid, using primer-pair 2126F/2129R and
608 PspOMI/MluI restriction sites. To avoid over-expression of the puromycin drug resistance marker, we
609 also eliminated the additional unmodified T7 RNAP promoter sequence contained in the plasmid
610 backbone by amplifying the whole expression cassette (using primer-pair 2067F/2068R) and cloning it
611 using PacI into the bacterial backbone of plasmid pTB007 (Beneke et al., 2017). We then cloned into
612 this resulting plasmid T7 RNAP and rRNAP promoter variant cassettes, containing tdTomato targeting
613 sgRNAs, by using again NsiI and MluI sites (primer-pairs 2014-2021 and 2025-2027). TdTomato-
614 targeting sgRNA expression constructs were then transfected as episomes into *L. major* parasites
615 that expressed a tdTomato reporter, T7 RNAP and CBE. Following transfection recovery, the
616 proportion of tdTomato-expressing cells was determined by FACS analysis and doubling times
617 measured. Transfection and FACS analysis were thereby carried out as described previously
618 (Engstler and Beneke, 2023). Following promoter testing, we then finalized our design and generated
619 pTB102 with a T7 RNAP T10 GG promoter variant (using primer-pair 2128F-T10GG/2129R).

620 To include homology flanks in the pTB102 plasmid, neomycin-targeting or 18S rRNA-targeting
621 regions were amplified and fused to pTB102 sgRNA expression cassettes using a fusion PCR
622 approach (primer-pairs 2236F-2257R). Resulting amplicons were cloned into PacI sites, resulting in
623 pTB104 (neomycin-targeting T7 RNAP expression plasmid) and pTB105 (18S rRNA-targeting T7
624 RNAP expression plasmid).

625 PF16 and tdTomato targeting CBE sgRNAs, as well as sgRNA libraries, were cloned into pTB102,
626 pTB104 and/or pTB105 plasmids using BbsI sites as previously described (Engstler and Beneke,
627 2023).

628 **Preparation of donor DNA and Cas12a crRNA template DNA**

629 To amplify the CBE sgRNA expression donor construct, 50 ng of plasmid template (pTB102, pTB104
630 or pTB105) containing a CBE targeting guide, 200 µM dNTPs, 0.5 µM each of forward and reverse

631 primers, and 1 unit of Q5 polymerase (New England Biolabs) were mixed in 1x Q5 buffer to a final
632 volume of 100 µl. Oligos used for amplification contained homology flanks of varying lengths. PCR
633 steps were 30 s at 98°C, followed by 20 cycles of 10 s at 98°C, 10 s at 65°C and 40 s at 72°C,
634 concluding with a final elongation step of 5 min at 72°C. Alternatively, donor DNA was produced by
635 digesting pTB104 and pTB105 plasmids with PacI. To confirm the presence of the expected product,
636 2 µl of this reaction was analysed on a 0.8% agarose gel.

637 For the amplification of the Cas12a crRNA template DNA, we used a common forward primer,
638 containing an unmodified T7 RNAP promoter sequence and an optimised Cas12a direct repeat (DR)
639 from DeWeirdt et al. (2021). For the PCR 200 µM dNTPs, 2 µM each of Cas12a forward primer and
640 corresponding reverse primer, and 1 unit of Phusion Polymerase (Thermo Fisher) were mixed in 1x
641 Phusion GC Buffer and 3 % DMSO to a total volume of 50 µl. PCR steps were 30 s at 98°C followed
642 by 35 cycles of 10 s at 98°C, 10 s at 65°C and 10s at 72° concluding with a final elongation step for 7
643 min at 72°C. Successful amplification was confirmed by running 2 µl of the reaction on a 2% agarose
644 gel.

645 The remainder of the donor and crRNA reaction was combined, EtOH purified, resuspended in 50 µl
646 ultra-pure water, heat sterilised at 95°C for 5 min and then used for transfection.

647 **Testing Cas12a-mediated integration of mNG constructs**

648 To test the Cas12a-mediated integration efficiency of donor DNA constructs with varying homology
649 flank lengths, we generated a DNA construct containing mNeonGreen (mNG) as a reporter and
650 blasticidin as a resistance marker, as well as ~600 nt homology flanks targeting the 18S rRNA SSU
651 locus (Misslitz et al., 2000; Sorensen et al., 2003). This construct was assembled by fusion PCR as
652 previously described (Engstler and Beneke, 2023), using pPLOT-mNG-Blast (Beneke et al., 2017) as
653 a PCR template. The generated fusion construct was then cloned into a blunted vector backbone,
654 resulting in the plasmid pPLOT-SSU-HDR-mNG-Blast.

655 We then PCR amplified as described above donor DNA from this plasmid with varying homology flank
656 lengths (~600 nt, 60 nt and 30 nt; Supplementary File 1). Resulting PCR amplicons and the pPLOT-
657 SSU-HDR-mNG-Blast plasmid itself were then purified using ethanol precipitation and normalized to
658 the same number of DNA molecules (3.6×10^{12} molecules per transfection). This normalization was
659 based on 10 µg of pPLOT-SSU-HDR-mNG-Blast plasmid. In addition, 10 µg of Cas12a crRNA
660 template DNA was added to donor DNA as indicated (Figure 2). As described previously (Engstler
661 and Beneke, 2023), DNA mixtures were then transfected using 5×10^{6} cells per transfection and we
662 determined the number of blasticidin resistant clones by immediately diluting transfected populations
663 and platting them on 96 well plates. In addition, 10 days post transfection undiluted blasticidin
664 resistant non-clonal populations were subjected to FACS analysis. To verify the correct integration of
665 donor DNA, DNA was isolated from these populations as described (Engstler and Beneke, 2023;
666 Rotureau et al., 2005) and amplified integration sites were submitted for Sanger sequencing at
667 Eurofins Genomics (Figure 2 S1A and D).

668 **High efficiency transfections**

669 Transfections were generally carried out as described in Engstler and Beneke (2023), transfecting
670 ~5×10^6 cells in 1x Tb-BSF buffer (Schumann Burkard et al., 2011) using 2 mm cuvettes (BTX) with an
671 Amaxa Nucleofector 2b (Lonza, program X-001).

672 For high efficiency transfections, we modified the protocol and compared side-by-side the transfection
673 efficiency of the Basic Parasite Nucleofector Kit (Lonza) and Tb-BSF protocol (Schumann Burkard et
674 al., 2011). 1×10^8 or 2.5×10^8 cells were collected, washed once in 1x Tb-BSF buffer and resuspended
675 in either 100 µl Lonza transfection reagent or 200 µl Tb-BSF buffer. 10 µg donor DNA and 10 µg
676 Cas12a crRNA template DNA were diluted in either 20 µl (Lonza transfection) or 50 µl (Tb-BSF
677 transfection) ultrapure water, heat sterilized and added to each transfection respectively (final
678 transfection volume Tb-BSF 250 µl, Lonza 120 µl). Cells were transfected using transfection cuvettes
679 supplied with the Basic Parasite Nucleofector Kit (Lonza transfection) or 2 mm BTX cuvettes (Tb-BSF
680 transfection) with one pulse of the X-001 program on an Amaxa Nucleofector 2b (Lonza). For
681 measuring transfection efficiencies, cells were selected and diluted on 96-well plates as described
682 (Engstler and Beneke, 2023).

683 **Small-scale loss-of-function screen**

684 For the small scale loss-of-functions screen, the CBE sgRNA pTB105 library was transfected as
685 described in the high efficiency transfections protocol above using 1×10^8 cells, 10 µg PacI-linearized
686 library DNA and 10 µg Cas12a crRNA template DNA. Six hours post transfection, non-clonal
687 transfected library populations were selected with 40 µg/ml Hygromycin B and 40 µg/ml Puromycin
688 Dihydrochloride. The transfection efficiency was determined as previously described (Engstler and
689 Beneke, 2023), yielding approximately one transfectant per 100 transfected cells. This corresponded
690 to a representation rate of ~25,000 cells per sgRNA within the transfected library. Cultures were
691 maintained for up to 288 hours with sub-cultures whenever the cell density reached 1×10^7 cells/ml. At
692 each time point, DNA was isolated from at least 1×10^7 cells, as described previously (Engstler and
693 Beneke, 2023; Rotureau et al., 2005). Then, 1 µg DNA from each time point and 10 ng DNA from
694 plasmid libraries were amplified using FastGene Optima HotStart Ready Mix (NIPPON; contains all
695 ingredients for PCR reaction). Amplification employed standard desalted p5 and p7 primers (Sigma,
696 Supplementary file 5), containing inline and i5/i7 barcodes for multiplexing, as well as adapters for
697 Illumina sequencing. Barcodes had a Hamming distance of at least 4nt. To avoid over-amplification,
698 samples isolated from transfected populations were amplified using 26 PCR cycles, while plasmid
699 samples were amplified using only 16 PCR cycles (ideal number of PCR cycles was assessed by
700 testing 12, 14, 16, 18 and 20 PCR cycles for plasmid samples and 22, 24, 26, 28, 30 and 32 PCR
701 cycles for samples isolated from transfected cells). Amplicons were pooled in equal ratios, size-
702 selected using SPRIselect beads (Beckman Coulter) and send to Novogene GmbH for partial-lane
703 Illumina sequencing (250 bp paired-end sequencing).

704 For analysis reads were de-multiplexed twice: first using bcl2fastq (Illumina) with i5 and i7 indices,
705 and then with cutadapt (Martin) using inline barcodes (with a 0.15 error rate). This double de-
706 multiplexing minimized index hopping. De-multiplexed forward reads were counted and normalized
707 using MAGeCK (Li et al., 2014). The ratio of normalized reads between plasmid (0 h) and each time
708 point post-transfection was calculated. A 0.99 confidence ellipse was generated based on non-
709 targeting control values alone (Supplementary File 4).

710 **Targeting of PF16 with an improved CBE system**

711 For testing the editing efficiency of our improved CBE system, we amplified donor DNA from the
712 pTB102 plasmid, containing the sgRNA PF16-3 from Engstler and Beneke (2023). As indicated
713 (Figure 4), donor DNAs were mixed with respective Cas12a crRNA DNA templates and transfected
714 into *Leishmania* parasites. Following selection and the recovery of parasites, non-clonal mutant
715 populations were tracked in duplicates or triplicates and their mean velocity determined as described
716 before (Engstler and Beneke, 2023). Editing rates were measured by amplifying the PF16 target locus
717 and by subjecting PCR amplicons to Sanger sequencing (Engstler and Beneke, 2023).

718 **ONT and Illumina sequencing analysis of CBE PF16 non-clonal mutant population**

719 DNA from *L. mexicana* CBE PF16 non-clonal mutant populations was isolated as previously
720 described (Engstler and Beneke, 2023; Rotureau et al., 2005) 16 days post transfection and
721 submitted for ONT and Illumina sequencing at Plasmidsaurus (service: “Big Hybrid ONT + Illumina”).
722 Obtained raw fastq files from ONT and Illumina sequencing were then assembled using the Burrows-
723 Wheeler Aligner (Li and Durbin, 2009) using two customized *L. mexicana* genomes of the
724 MHOMGT2001U1103 annotation. In the first genome, we duplicated chromosome 27 and modified
725 the 18S rRNA SSU locus of one chromosome 27 copy to include the tdTomato expression cassette
726 (Engstler and Beneke, 2023) (Figure 4 S1B), while the other copy contained the CBE sgRNA
727 expression construct. In the second genome, we instead modified chromosome 27 to contain both
728 expression cassettes consecutively (Figure 4 S1C). Following alignments, we then used samtools (Li
729 et al., 2009) for sorting and indexing of bam files and viewed our analysis using the IGV genome
730 browser (Robinson et al., 2011). ONT and Illumina fastq reads are available at the European
731 Nucleotide Archive (ENA) (Accession number: PRJEB83088).

732 For the standard nucleotide BLAST analysis (Altschul et al., 1990), ONT fastq reads were queried
733 against the coding sequence of the tdTomato reporter gene and the sgRNA expression cassette. The
734 cassette included the optimized T7 RNAP promoter (T7 T10 GG), PF16-3 targeting spacer, and Cas9
735 sgRNA scaffold sequence. Extracted contigs were then mapped to the 18S rRNA integration locus
736 and adjacent genomic sites using Clustal Omega (Sievers et al., 2011).

737 **Optimised CBE sgRNA scoring**

738 To determine the likelihood of successful gene editing, we adjusted the sgRNA ranking system. New
739 sgRNA ranking scores were calculated based on various parameters, including the relative likelihood

740 of generating a STOP codon from a cytosine base, the total number of possible STOP codons, the
741 location of cytosines within the editing window, and the position of the guide's target within the coding
742 sequence (CDS) of the gene. To generate the overall score, we weighted the contribution of each of
743 these scores, with the likelihood of generating a stop codon having four times more contribution than
744 the other scores. We then normalized the total score on a scale of 0 to 100, where 0 represents the
745 best score, and 100 represents the worst score.

746 The updated data sets and code can be accessed at http://www.leishbaseedit.net/ and
747 https://github.com/ElisabethMeiser/Collaboration_Beneke_Meiser, respectively.

748 **Cas12a-mediated gene replacement for generation of knockout cell lines**

749 For the Cas12a-mediated replacement of the PF16 CDS, we adapted the LeishGEdit approach
750 (Beneke and Gluenz, 2019; Beneke and Gluenz, 2020; Beneke et al., 2017) and PCR-amplified two
751 Cas12a crRNAs targeting the 5' and 3' UTR of the PF16 ORF (crRNA design as described above). In
752 addition, we PCR-amplified pTBlast and pTPuro cassettes from the LeishGEdit toolbox with primers
753 containing 30 nt homology flanks adjacent to these crRNAs. Both types of PCR were carried out as
754 described above and we then co-transfected all resulting products into *L. mexicana* cells containing
755 the pTB107 plasmid. Successful gene replacement in obtained non-clonal mutant populations was
756 confirmed by amplifying and Sanger sequencing the PF16 locus with two ORF spanning primers.

757

AVAILABILITY

All data generated or analyzed during this study are included in the manuscript and supplementary files. LeishBASEedit is an open-source primer design tool accessible at www.leishbaseedit.net. Plasmids pTB102, pTB104, pTB105, pTB106, and pTB107 can be requested through the LeishBASEedit platform and will also be made available on Addgene in the near future. ONT and Illumina fastq reads are available at ENA (Accession number: PRJEB83088).

ACKNOWLEDGEMENT

We thank all members of the Alsheimer, Engstler, Janzen and Kramer group for helpful discussions and support. In addition, we thank Markus Engstler for providing research resources and helpful comments on the manuscript. We thank Ger van Zandbergen from the Paul-Ehrlich-Institut for his support in acquiring funding for JA and FL, who were supported by a Flex fund within the LOEWE Center DRUID (Project D3, B3). TB and NHM were supported by the DFG (project 532631727). Additionally, TB was supported by an EMBO Postdoctoral Fellowship (ALTF 727-2021) and Marie Skłodowska-Curie Actions Postdoctoral Fellowship (101064428 – LeishMOM).

CONFLICT OF INTEREST

All authors declare that they have no conflicts of interest.

774 **REFERENCES**

775 **Alsford, S., Turner, D. J., Obado, S. O., Sanchez-Flores, A., Glover, L., Berriman, M., Hertz-**
776 **Fowler, C. and Horn, D.** (2011). High-throughput phenotyping using parallel sequencing of RNA
777 interference targets in the African trypanosome. *Genome Res* **21**, 915-24.
778 **Altschul, S. F., Gish, W., Miller, W., Myers, E. W. and Lipman, D. J.** (1990). Basic local
779 alignment search tool. *J Mol Biol* **215**, 403-10.
780 **Ariyanayagam, M. R., Oza, S. L., Guther, M. L. and Fairlamb, A. H.** (2005). Phenotypic
781 analysis of trypanothione synthetase knockdown in the African trypanosome. *Biochem J* **391**, 425-32.
782 **Aslett, M., Aurrecoechea, C., Berriman, M., Brestelli, J., Brunk, B. P., Carrington, M.,**
783 **Depledge, D. P., Fischer, S., Gajria, B., Gao, X. et al.** (2010). TriTrypDB: a functional genomic
784 resource for the Trypanosomatidae. *Nucleic Acids Res* **38**, D457-62.
785 **Baker, N., Catta-Preta, C. M. C., Neish, R., Sadlova, J., Powell, B., Alves-Ferreira, E. V. C.,**
786 **Geoghegan, V., Carnielli, J. B. T., Newling, K., Hughes, C. et al.** (2021). Systematic functional analysis
787 of Leishmania protein kinases identifies regulators of differentiation or survival. *Nat Commun* **12**,
788 1244.
789 **Beneke, T., Demay, F., Hookway, E., Ashman, N., Jeffery, H., Smith, J., Valli, J., Becvar, T.,**
790 **Myskova, J., Lestinova, T. et al.** (2019). Genetic dissection of a Leishmania flagellar proteome
791 demonstrates requirement for directional motility in sand fly infections. *PLoS Pathog* **15**, e1007828.
792 **Beneke, T., Dobramysl, U., Catta-Preta, C. M. C., Mottram, J. C., Gluenz, E. and Wheeler, R.**
793 **J.** (2022). Genome sequence of Leishmania mexicana MNYC/BZ/62/M379 expressing Cas9 and T7
794 RNA polymerase. *Wellcome Open Res* **7**, 294.
795 **Beneke, T. and Gluenz, E.** (2019). LeishGEdit: A Method for Rapid Gene Knockout and
796 Tagging Using CRISPR-Cas9. *Methods Mol Biol* **1971**, 189-210.
797 **Beneke, T. and Gluenz, E.** (2020). Bar-seq strategies for the LeishGEdit toolbox. *Mol Biochem*
798 *Parasitol* **239**, 111295.
799 **Beneke, T., Madden, R., Makin, L., Valli, J., Sunter, J. and Gluenz, E.** (2017). A CRISPR Cas9
800 high-throughput genome editing toolkit for kinetoplastids. *R Soc Open Sci* **4**, 170095.
801 **Beneke, T., Neish, R., Catta-Preta, C. M. C., Smith, J., Valli, J., McCoy, C., Albuquerque-**
802 **Wendt, A., Mottram, J. C. and Gluenz, E.** (2024). IFT and BBSome proteins are required for
803 Leishmania mexicana pathogenicity, but flagellar motility is dispensable. *bioRxiv*.
804 **Burge, R. J., Damianou, A., Wilkinson, A. J., Rodenko, B. and Mottram, J. C.** (2020).
805 Leishmania differentiation requires ubiquitin conjugation mediated by a UBC2-UEV1 E2 complex.
806 *PLoS Pathog* **16**, e1008784.
807 **Burkard, G., Fragoso, C. M. and Roditi, I.** (2007). Highly efficient stable transformation of
808 bloodstream forms of Trypanosoma brucei. *Mol Biochem Parasitol* **153**, 220-3.
809 **Chhajer, R., Bhattacharyya, A., Didwania, N., Shadab, M., Das, N., Palit, P., Vaidya, T. and**
810 **Ali, N.** (2016). Leishmania donovani Aurora kinase: A promising therapeutic target against visceral
811 leishmaniasis. *Biochim Biophys Acta* **1860**, 1973-88.
812 **Damianou, A., Burge, R. J., Catta-Preta, C. M. C., Geoghegan, V., Nievas, Y. R., Newling, K.,**
813 **Brown, E., Burchmore, R., Rodenko, B. and Mottram, J. C.** (2020). Essential roles for
814 deubiquitination in Leishmania life cycle progression. *PLoS Pathog* **16**, e1008455.
815 **de Paiva, R. M., Grazielle-Silva, V., Cardoso, M. S., Nakagaki, B. N., Mendonca-Neto, R. P.,**
816 **Canavaci, A. M., Souza Melo, N., Martinelli, P. M., Fernandes, A. P., daRocha, W. D. et al.** (2015).
817 Amastin Knockdown in Leishmania braziliensis Affects Parasite-Macrophage Interaction and Results
818 in Impaired Viability of Intracellular Amastigotes. *PLoS Pathog* **11**, e1005296.
819 **Decuypere, S., Rijal, S., Yardley, V., De Doncker, S., Laurent, T., Khanal, B., Chappuis, F. and**
820 **Dujardin, J. C.** (2005). Gene expression analysis of the mechanism of natural Sb(V) resistance in
821 Leishmania donovani isolates from Nepal. *Antimicrob Agents Chemother* **49**, 4616-21.

822 **DeWeirdt, P. C., Sanson, K. R., Sangree, A. K., Hegde, M., Hanna, R. E., Feeley, M. N.,**
823 **Griffith, A. L., Teng, T., Borys, S. M., Strand, C. et al.** (2021). Optimization of AsCas12a for
824 combinatorial genetic screens in human cells. *Nat Biotechnol* **39**, 94-104.
825 **Doench, J. G., Fusi, N., Sullender, M., Hegde, M., Vaimberg, E. W., Donovan, K. F., Smith, I.,**
826 **Tothova, Z., Wilen, C., Orchard, R. et al.** (2016). Optimized sgRNA design to maximize activity and
827 minimize off-target effects of CRISPR-Cas9. *Nat Biotechnol* **34**, 184-191.
828 **Duncan, S. M., Myburgh, E., Philipon, C., Brown, E., Meissner, M., Brewer, J. and Mottram,**
829 **J. C.** (2016). Conditional gene deletion with DiCre demonstrates an essential role for CRK3 in
830 Leishmania mexicana cell cycle regulation. *Mol Microbiol* **100**, 931-44.
831 **Engstler, M. and Beneke, T.** (2023). Gene editing and scalable functional genomic screening
832 in Leishmania species using the CRISPR/Cas9 cytosine base editor toolbox LeishBASEedit. *Elife* **12**.
833 **Gier, R. A., Budinich, K. A., Evitt, N. H., Cao, Z., Freilich, E. S., Chen, Q., Qi, J., Lan, Y., Kohli,**
834 **R. M. and Shi, J.** (2020). High-performance CRISPR-Cas12a genome editing for combinatorial genetic
835 screening. *Nat Commun* **11**, 3455.
836 **Glover, L., Alsford, S., Baker, N., Turner, D. J., Sanchez-Flores, A., Hutchinson, S., Hertz-**
837 **Fowler, C., Berriman, M. and Horn, D.** (2015). Genome-scale RNAi screens for high-throughput
838 phenotyping in bloodstream-form African trypanosomes. *Nat Protoc* **10**, 106-33.
839 **Glover, L. and Horn, D.** (2009). Site-specific DNA double-strand breaks greatly increase
840 stable transformation efficiency in Trypanosoma brucei. *Mol Biochem Parasitol* **166**, 194-7.
841 **Hassan, P., Fergusson, D., Grant, K. M. and Mottram, J. C.** (2001). The CRK3 protein kinase is
842 essential for cell cycle progression of Leishmania mexicana. *Mol Biochem Parasitol* **113**, 189-98.
843 **Horn, D.** (2022). Genome-scale RNAi screens in African trypanosomes. *Trends Parasitol* **38**,
844 160-173.
845 **Labuhn, M., Adams, F. F., Ng, M., Knoess, S., Schambach, A., Charpentier, E. M., Schwarzer,**
846 **A., Mateo, J. L., Klusmann, J. H. and Heckl, D.** (2018). Refined sgRNA efficacy prediction improves
847 large- and small-scale CRISPR-Cas9 applications. *Nucleic Acids Res* **46**, 1375-1385.
848 **Li, H. and Durbin, R.** (2009). Fast and accurate short read alignment with Burrows-Wheeler
849 transform. *Bioinformatics* **25**, 1754-60.
850 **Li, H., Handsaker, B., Wysoker, A., Fennell, T., Ruan, J., Homer, N., Marth, G., Abecasis, G.,**
851 **Durbin, R. and Genome Project Data Processing, S.** (2009). The Sequence Alignment/Map format
852 and SAMtools. *Bioinformatics* **25**, 2078-9.
853 **Li, W., Xu, H., Xiao, T., Cong, L., Love, M. I., Zhang, F., Irizarry, R. A., Liu, J. S., Brown, M.**
854 **and Liu, X. S.** (2014). MAGeCK enables robust identification of essential genes from genome-scale
855 CRISPR/Cas9 knockout screens. *Genome Biol* **15**, 554.
856 **Lye, L. F., Owens, K., Shi, H., Murta, S. M., Vieira, A. C., Turco, S. J., Tschudi, C., Ullu, E. and**
857 **Beverley, S. M.** (2010). Retention and loss of RNA interference pathways in trypanosomatid
858 protozoans. *PLoS Pathog* **6**, e1001161.
859 **Lye, L. F., Owens, K. L., Jang, S., Marcus, J. E., Brettmann, E. A. and Beverley, S. M.** (2022).
860 An RNA Interference (RNAi) Toolkit and Its Utility for Functional Genetic Analysis of Leishmania
861 (Viannia). *Genes (Basel)* **14**.
862 **Madeira da Silva, L. and Beverley, S. M.** (2010). Expansion of the target of rapamycin (TOR)
863 kinase family and function in Leishmania shows that TOR3 is required for acidocalcisome biogenesis
864 and animal infectivity. *Proc Natl Acad Sci U S A* **107**, 11965-70.
865 **Martel, D., Beneke, T., Gluenz, E., Spath, G. F. and Rachidi, N.** (2017). Characterisation of
866 Casein Kinase 1.1 in Leishmania donovani Using the CRISPR Cas9 Toolkit. *Biomed Res Int* **2017**,
867 4635605.
868 **Martin, M.** Cutadapt Removes Adapter Sequences From High-Throughput Sequencing Reads.
869 *EMBnet.journal Bioinformatic in Action* **17**.
870 **Misslitz, A., Mottram, J. C., Overath, P. and Aebischer, T.** (2000). Targeted integration into a
871 rRNA locus results in uniform and high level expression of transgenes in Leishmania amastigotes.
872 *Mol Biochem Parasitol* **107**, 251-61.

873 **Morris, J. C., Wang, Z., Drew, M. E. and Englund, P. T.** (2002). Glycolysis modulates
874 trypanosome glycoprotein expression as revealed by an RNAi library. *EMBO J* **21**, 4429-38.
875 **Padmanabhan, R., Sarcar, S. N. and Miller, D. L.** (2020). Promoter Length Affects the
876 Initiation of T7 RNA Polymerase In Vitro: New Insights into Promoter/Polymerase Co-evolution. *J Mol*
877 *Evol* **88**, 179-193.
878 **Passos-Silva, D. G., Rajao, M. A., Nascimento de Aguiar, P. H., Vieira-da-Rocha, J. P.,**
879 **Machado, C. R. and Furtado, C.** (2010). Overview of DNA Repair in Trypanosoma cruzi, Trypanosoma
880 brucei, and Leishmania major. *J Nucleic Acids* **2010**, 840768.
881 **Paul, B. and Montoya, G.** (2020). CRISPR-Cas12a: Functional overview and applications.
882 *Biomed J* **43**, 8-17.
883 **Queffeulou, M., Leprohon, P., Fernandez-Prada, C., Ouellette, M. and Mejia-Jaramillo, A.**
884 **M.** (2024). CRISPR-Cas9 high-throughput screening to study drug resistance in Leishmania infantum.
885 *MBio* **15**, e0047724.
886 **Rachidi, N., Taly, J. F., Durieu, E., Leclercq, O., Aulner, N., Prina, E., Pescher, P., Notredame,**
887 **C., Meijer, L. and Spath, G. F.** (2014). Pharmacological assessment defines Leishmania donovani
888 casein kinase 1 as a drug target and reveals important functions in parasite viability and intracellular
889 infection. *Antimicrob Agents Chemother* **58**, 1501-15.
890 **Rastogi, R., Verma, J. K., Kapoor, A., Langsley, G. and Mukhopadhyay, A.** (2016). Rab5
891 Isoforms Specifically Regulate Different Modes of Endocytosis in Leishmania. *J Biol Chem* **291**, 14732-
892 46.
893 **Robinson, J. T., Thorvaldsdottir, H., Winckler, W., Guttman, M., Lander, E. S., Getz, G. and**
894 **Mesirov, J. P.** (2011). Integrative genomics viewer. *Nat Biotechnol* **29**, 24-6.
895 **Rotureau, B., Gego, A. and Carme, B.** (2005). Trypanosomatid protozoa: a simplified DNA
896 isolation procedure. *Exp Parasitol* **111**, 207-9.
897 **Sanjana, N. E., Shalem, O. and Zhang, F.** (2014). Improved vectors and genome-wide
898 libraries for CRISPR screening. *Nat Methods* **11**, 783-784.
899 **Schlecker, T., Schmidt, A., Dirdjaja, N., Voncken, F., Clayton, C. and Krauth-Siegel, R. L.**
900 (2005). Substrate specificity, localization, and essential role of the glutathione peroxidase-type
901 tryparedoxin peroxidases in Trypanosoma brucei. *J Biol Chem* **280**, 14385-94.
902 **Schumann Burkard, G., Jutzi, P. and Roditi, I.** (2011). Genome-wide RNAi screens in
903 bloodstream form trypanosomes identify drug transporters. *Mol Biochem Parasitol* **175**, 91-4.
904 **Schumann, G., Kangussu-Marcolino, M. M., Doiron, N., Kaser, S., de Assis Burle-Caldas, G.,**
905 **DaRocha, W. D., Teixeira, S. M. and Roditi, I.** (2017). Zinc finger nuclease technology: A stable tool
906 for high efficiency transformation in bloodstream form T. brucei. *Mol Biochem Parasitol* **213**, 12-15.
907 **Sievers, F., Wilm, A., Dineen, D., Gibson, T. J., Karplus, K., Li, W., Lopez, R., McWilliam, H.,**
908 **Remmert, M., Soding, J. et al.** (2011). Fast, scalable generation of high-quality protein multiple
909 sequence alignments using Clustal Omega. *Mol Syst Biol* **7**, 539.
910 **Sorensen, M., Lippuner, C., Kaiser, T., Misslitz, A., Aebischer, T. and Bumann, D.** (2003).
911 Rapidly maturing red fluorescent protein variants with strongly enhanced brightness in bacteria.
912 *FEBS Lett* **552**, 110-4.
913 **Stemmer, M., Thumberger, T., Del Sol Keyer, M., Wittbrodt, J. and Mateo, J. L.** (2015).
914 CCTop: An Intuitive, Flexible and Reliable CRISPR/Cas9 Target Prediction Tool. *PLoS One* **10**,
915 e0124633.
916 **Sunter, J. D., Moreira-Leite, F. and Gull, K.** (2018). Dependency relationships between IFT-
917 dependent flagellum elongation and cell morphogenesis in Leishmania. *Open Biol* **8**.
918 **Ullu, E., Tschudi, C. and Chakraborty, T.** (2004). RNA interference in protozoan parasites.
919 *Cell Microbiol* **6**, 509-19.
920 **Wirtz, E., Hoek, M. and Cross, G. A.** (1998). Regulated processive transcription of chromatin
921 by T7 RNA polymerase in Trypanosoma brucei. *Nucleic Acids Res* **26**, 4626-34.

922 **Yagoubat, A., Crobu, L., Berry, L., Kuk, N., Lefebvre, M., Sarrazin, A., Bastien, P. and**
923 **Sterkers, Y.** (2020). Universal highly efficient conditional knockout system in Leishmania, with a
924 focus on untranscribed region preservation. *Cell Microbiol* **22**, e13159.
925 **Yau, E. H. and Rana, T. M.** (2018). Next-Generation Sequencing of Genome-Wide CRISPR
926 Screens. *Methods Mol Biol* **1712**, 203-216.
927 **Zhang, L., Zuris, J. A., Viswanathan, R., Edelstein, J. N., Turk, R., Thommandru, B., Rube, H.**
928 **T., Glenn, S. E., Collingwood, M. A., Bode, N. M. et al.** (2021). AsCas12a ultra nuclease facilitates the
929 rapid generation of therapeutic cell medicines. *Nat Commun* **12**, 3908.
930 **Zhang, W. W., Lypaczewski, P. and Matlashewski, G.** (2017). Optimized CRISPR-Cas9
931 Genome Editing for Leishmania and Its Use To Target a Multigene Family, Induce Chromosomal
932 Translocation, and Study DNA Break Repair Mechanisms. *mSphere* **2**.
933 **Zhang, W. W. and Matlashewski, G.** (2015). CRISPR-Cas9-Mediated Genome Editing in
934 Leishmania donovani. *MBio* **6**, e00861.
935 **Zhang, W. W. and Matlashewski, G.** (2019). Single-Strand Annealing Plays a Major Role in
936 Double-Strand DNA Break Repair following CRISPR-Cas9 Cleavage in Leishmania. *mSphere* **4**.
937 **Zhang, W. W., Wright, D. G., Harrison, L. and Matlashewski, G.** (2022). Reconstitution of
938 Mycobacterium marinum Nonhomologous DNA End Joining Pathway in Leishmania. *mSphere* **7**,
939 e0015622.
940 **Zhang, X., Chen, L., Zhu, B., Wang, L., Chen, C., Hong, M., Huang, Y., Li, H., Han, H., Cai, B.**
941 **et al.** (2020). Increasing the efficiency and targeting range of cytidine base editors through fusion of
942 a single-stranded DNA-binding protein domain. *Nat Cell Biol* **22**, 740-750.

943

944 **FIGURE LEGENDS**

945 **Figure 1. Optimisation of CBE sgRNA expression in *L. major*.** Schematics of base editing
946 strategies to transfect *Leishmania* parasites either with a (**A**) single or (**B**) dual base editing system.
947 (**A**) Plasmid pLdCH-hyBE4max (Engstler and Beneke, 2023) contains (from left to right) a
948 *L. donovani*-derived ribosomal RNA (rRNA) promoter, single-guide RNA (sgRNA) expression cassette,
949 hepatitis delta virus (HDV) ribozyme containing transsplice sequence (TSS), hyBE4max CBE,
950 *L. donovani*-derived A2 intergenic sequence, and hygromycin resistance marker. (**B**) Plasmid
951 pTB007-hyBE4max (Engstler and Beneke, 2023) contains separated through intergenic regions (from
952 left to right) a hyBE4max CBE, T7 RNAP and hygromycin resistance marker. This construct is
953 integrated into the β-tubulin locus of *L. major* parasites (LmjF.33:339,096–341,104). The CBE sgRNA
954 expression vector contains a puromycin resistance marker, T7 RNAP promoter, single-guide RNA
955 (sgRNA) expression cassette and HDV ribozyme. (**C**) Different versions of the T7 RNAP promoter for
956 CBE sgRNA expression have been tested. (**D**) Doubling times of tdTomato-expressing *L. major*
957 transfected non-clonal populations with the single plasmid system and variants of the dual plasmid
958 system for targeting of tdTomato. Error bars show standard deviations of triplicates. Tar: Cells
959 transfected with a CBE sgRNA expression plasmid that facilitates the introduction of a STOP codon
960 within the tdTomato ORF; Ctrl: Cells transfected with a CBE sgRNA expression plasmid that causes a
961 codon mutation without amino acid change. Asterisks indicate Student's t-test: *p > 0.05. (**E**) FACS
962 plot of parasites shown in (**D**), analysed 7 days post transfection. (**F**) FACS plot showing tdTomato-
963 expressing and wildtype *L. major* parasites.

964 **Figure 2. Developing an AsCas12a-mediated integration system.** (**A**) Schematic of the Cas12a-
965 mediated integration approach. A stable *L. mexicana* cell line maintains plasmid pTB107 as an
966 episome and is co-transfected with a donor DNA reporter construct and a Cas12a crRNA template
967 DNA. Using a T7 RNAP promoter, the Cas12a crRNA template DNA is *in vivo* transcribed to facilitate
968 a Cas12a-mediated DSB at the 18S rRNA SSU locus. Using homology flanks the reporter construct is
969 efficiently integrated at the site of the DSB. Plasmid pTB107 thereby allows for the expression of
970 hyBE4max CBE, AsCas12a ultra (Zhang et al., 2021), T7 RNAP and hygromycin resistance marker.
971 AsCas12a ultra and T7 RNAP are expressed as a fusion protein but then cleaved through a P2A self-
972 cleaving peptide. The reporter constructs consists of a pPLOT plasmid tagging cassette (Beneke et
973 al., 2017) with additional homology flanks, allowing for the expression of mNeonGreen and a
974 blasticidin resistance marker. (**B**) Schematic of the Cas12a crRNA template DNA generation. Two
975 overlapping primers are amplified in a PCR reaction. The forward primer is common and contains an
976 unmodified T7 RNAP promoter and an optimised Cas12a direct repeat variant (DR) (DeWeirdt et al.,
977 2021). The guide reverse primer contains the crRNA specific spacer sequence aligning to the
978 targeted locus and the Cas12a DR to enable the overlap with the forward primer. (**C** and **E**) FACS plot
979 showing *L. mexicana* pTB107 non-clonal populations following the transfection described in (**A**).
980 Percentages represent the remaining proportion of mNeonGreen-expressing cells. (**C**) The homology
981 flank (HF) length used for reporter construct integration has been varied and the additional use of
982 Cas12a crRNA was tested. The transfection of a circular plasmid, containing the reporter construct

983 was included as a control (episomal). (**E**) Six different Cas12a crRNAs have been tested using two
984 different integration loci (as described in the main text). (**D** and **F**) Efficiency of transfections shown in
985 (**C** and **E**) were measured. The number of cells required for the transfection to obtain one transfectant
986 is shown. Error bars show standard deviations of triplicates.

987 **Figure 2 S1. Verification of AsCas12a-mediated reporter construct integration.** (**A**) Locus map of
988 the 18S rRNA SSU locus in *L. mexicana pTB107* cells before and after co-transfection of Cas12a
989 crRNA-1 and a reporter construct (as described in Figure 2A, C and D). The positions of Cas12a
990 crRNA-1 and HFs used for the integration of the reporter are highlighted. Amplicons of PCR reactions
991 spanning the integration sites are indicated and amplification results are shown in (**B**), with DNA sizes
992 highlighted in bp. (**C**) Sanger sequencing trace plots of amplicons from non-clonal populations shown
993 in (**B**). The site of integration into the 18S rRNA locus is highlighted with a dotted line. (**D**) Locus map
994 of the 18S rRNA SSU locus in *L. mexicana pTB107* cells expressing tdTomato before and after co-
995 transfection of various Cas12a crRNAs and a reporter construct (as described in Figure 2A, E and F).
996 The positions of Cas12a crRNA-1, 2, 3, 4, 5 and 6 are highlighted. Indicated HF positions have been
997 used for the integration of the tdTomato expression construct on one allele but individual HFs
998 adjacent to crRNA-1 to 6 have been used for integration of the reporter construct. Amplicons of PCR
999 reactions spanning the integration sites are indicated and amplification results are shown in (**E**) for
1000 verification of crRNA-4. (**F**) Sanger sequencing trace plots of amplicons from non-clonal populations
1001 shown in (**E**).

1002 **Figure 3. Integration of CBE sgRNA expression cassettes via AsCas12a ultra.** (**A**) Schematic of
1003 Cas12a-mediated integration of the CBE sgRNA expression construct. The pTB107 stable cell line is
1004 co-transfected with two constructs: (1) a Cas12a crRNA template DNA and (2) a CBE sgRNA
1005 expression construct. The Cas12a crRNA template DNA is *in vivo* transcribed and consists of an
1006 unmodified T7 RNAP promoter (T7wt, light green), a Cas12a direct repeat (DR, red) and a 20 nt
1007 Cas12a guide target sequence (SPACER, blue). The CBE sgRNA expression construct is integrated
1008 into the 18s rRNA SSU locus, following the Cas12a-mediated DSB. This donor construct contains two
1009 homology flanks (HF, yellow), a puromycin-resistance marker (grey), a T7 T-10 GG promoter (green),
1010 a guide target sequence (orange), a Cas9 scaffold (dark green) and an HDV (purple). (**B**) FACS plots
1011 show pTB107 parasites that express tdTomato and have been transfected with pTB104 and pTB105
1012 CBE sgRNA expression cassettes, containing a tdTomato-targeting guide. Percentages represent the
1013 remaining proportion of non-clonal tdTomato-expressing cells. (**C**) Following dilutions after
1014 transfection, the number of puromycin-resistant transfectants obtained per transfected cell was
1015 calculated. Error bars show standard deviations of triplicates. (**D**) Doubling times for transfected
1016 *Leishmania* parasites shown in (**B**). PAR: parental cell line, UT: Un-transfected control.

1017 **Figure 4. Targeting PF16 via Cas12a-delivered CBE sgRNA expression cassettes.** *L. major*, *L.*
1018 *mexicana*, *L. donovani* wildtype and tdTomato/pTB107 cell lines were transfected with a range of CBE
1019 sgRNA expression constructs in order to functionally mutate PF16. Different strategies for construct
1020 delivery and sgRNA expression were tested, including the integration of constructs into the neomycin-
1021 resistance marker (using Cas12a sgRNA-6) and the 18S rRNA SSU locus (Cas12a sgRNA-4), each

using 60 nt homology flanks. For comparison to our previous system (Engstler and Beneke, 2023), we also expressed CBE sgRNAs from an episome and transfected pLdCH-hyBE4max into *L. major*. (**A**) Violin plot of pooled replicates from motility tracked non-clonal populations. The mean velocity of tracked cells was plotted 14 days post transfection for *L. major*, and 6 and 16 days post transfection for *L. mexicana* and *L. donovani*. The total percentage of tracked cells showing a velocity of less than 1 µm/s is highlighted. Each population was analysed using a Cramér-von Mises Test to detect any shift in the population distribution towards lower speed. Percentages are marked with an asterisks when that shift was significant (*p > 0.05). (**B**) Corresponding Sanger sequencing trace plots. Blue shading: 20 nt guide target sequence. Red dotted lines: hyBE4max editing window.

Figure 4 S1. ONT and Illumina sequencing of non-clonal transfectants. *L. mexicana* pTB107 cells expressing tdTomato were co-transfected with Cas12a crRNA-4 template DNA constructs and a CBE sgRNA expression cassette containing a PF16 targeting guide sequence. Isolated DNA from non-clonal mutant populations were subjected to ONT and Illumina sequencing 16 days post transfection. (**A**) Illumina sequencing reads were mapped against the *L. mexicana* MHOMGT2001U1103 genome annotation. The edited consensus sequence is shown alongside with the reference sequence and calculated editing rates (based on 35× genome coverage). (**B** and **C**) ONT reads were mapped against two customized *L. mexicana* MHOMGT2001U1103 genome annotations and viewed in the IGV genome browser (Robinson et al., 2011), with uniquely mapped reads in grey and reads with multiple alignments in white. Reads mapped against the PGKB 5' and 3'UTR are over-represented as these UTRs are also present in the pTB107 plasmid. (**B**) ONT reads were mapped to a customized genome in which we assumed that the 18S rRNA SSU locus had one integrated copy of the tdTomato expression cassette on one allele and one integrated copy of the CBE sgRNA expression construct on the other allele. Schematics show the annotation of genetic elements assumed to be on each allele. The position of one allele in respect to the position on the other allele is indicated with red arrows. The position of the Cas12a crRNA-4 to integrate the CBE sgRNA expression cassette is additionally highlighted. Black arrows indicate unique ONT reads that cover the entire customized locus. Reads are trimmed as the genome annotation is incomplete (NNN gap highlighted). (**C**) ONT reads were mapped to a customized genome in which we assumed that both cassettes were integrated on the same allele and could be detected on a single ONT read. (**D**) Illumina read coverage was normalized and chromosome coverage was compared to coverage of individual genetic features on these chromosomes.

Figure 4 S2. Blast analysis of ONT sequencing. (**A**) Schematic of tdTomato and CBE sgRNA expression cassette integration into the 18S rRNA locus. (**B**) Overview of the standard nucleotide Blast search process, where ONT fastq reads were queried against the coding sequences of the tdTomato reporter gene and the sgRNA expression cassette. (**C** and **D**) Alignment of matched ONT reads against the 18S rRNA locus, confirming that contigs correspond to the integration site and adjacent genomic sequences. The IDs for each matching contig are provided, and the data are available at the ENA (Accession number: PRJEB83088).

1060 **Figure 4 S3. Sequencing of clones isolated from an AsCas12a-mediated library transfection.**
1061 *L. mexicana*, *L. major* and *L. donovani* tdTomato/pTB107 cell lines were co-transfected with a library
1062 containing a mixtures of 15 guides and Cas12a crRNA-4 targeting the 18S rRNA SSU locus. Library
1063 clones from library transfection were isolated and their CBE sgRNA amplified for Sanger sequencing.
1064 (**A**) Sanger sequencing trace plots of the library before and 6 days post transfection. The T7 T10 GG
1065 promoter, sgRNA target sequence and the beginning of the sgRNA scaffold sequence are highlighted.
1066 (**B**) Sanger sequencing trace plots of guide cassettes sequenced from clones. Highlighted in red are
1067 clones that maintain more than one sgRNA.

1068 **Figure 4 S4. Novel scoring for CBE sgRNA sorting.** Schematic of new CBE scoring matrix. A
1069 sgRNA receives the highest score, when the ratio of available cytosines to resulting STOP codons is
1070 1:1. Additionally, the final score depends on the number of possible STOP codons and position of
1071 cytosines within the editing window (activities indicated above: high, mid and low).

1072 **Figure 5. Small scale loss-of-function screen.** (**A**) Cas12a-mediated integration of the CBE sgRNA
1073 expression construct library involves co-transfecting a cell line expressing tdTomato and containing
1074 either pTB107 or pTB106 with two constructs: (1) a Cas12a crRNA template DNA and (2) a CBE
1075 sgRNA expression construct library. Integration is facilitated by Cas12a-mediated DSBs, as described
1076 in Figure 3. (**B**) The library, transfected in three independent replicates, contains 15 non-targeting
1077 sgRNAs and 24 sgRNAs targeting essential or fitness-associated genes. Plasmid library DNA and
1078 genomic DNA from transfected cells were extracted before transfection (0 hours) and after several
1079 sub-cultures (168, 216, and 288 hours post-transfection). (**C**) Samples underwent Illumina amplicon
1080 sequencing for downstream analysis. (**D** and **E**) For each sgRNA, the ratio of normalized counts
1081 between 0h and 168, 216, or 288h was calculated and plotted against raw read counts. Averages
1082 from triplicates are displayed with error bars indicating the standard deviation. A 0.99 confidence
1083 ellipse, calculated from non-targeting controls, highlights significant sgRNA depletion when data
1084 points fall outside the ellipse. CBEs used in the screen differ in the RAD51 single-stranded DNA-
1085 binding domain within the hyBE4max enzyme, derived from either *L. major* (pTB106: *L.m.* RAD51-BD)
1086 or *Homo sapiens* (pTB107: *H.s.* RAD51-BD). (**E**) For the comparison, data from Engstler and Beneke
1087 (2023) (LeishBASEedit v1) were re-analysed and plotted alongside the newly generated data from
1088 this study (LeishBASEedit v2).

1089 **Figure 6. PF16 gene replacement by using CRISPR/AsCas12a ultra.** (**A**) Map of the PF16 locus
1090 before and after targeting with Cas12a 5' and 3'crRNA positions indicated. The PF16-ORF is replaced
1091 with a pTBlast and pTPuro cassette. Primers used for verification of the ORF replacement are
1092 highlighted with PCR amplicon length. (**B**) Visualization of PCR amplicons, showing expected
1093 products for pTPuro and pTBlast in the ΔPF16 lane and the amplicon of the PF16-ORF in the
1094 PARENT lane (*L. mexicana* tdTomato/pTB107 cell line). (**C** and **D**) Sanger sequencing trace plots of
1095 amplicons in (**B**), showing sequencing of the upstream region in (**C**) and downstream region in (**D**).
1096 Black arrows indicate Cas12a DSBs. (**E**) Violin plot of pooled replicates from motility tracked non-
1097 clonal populations, including the ΔPF16 and PARENT cell line. The total percentage of tracked cells
1098 showing a velocity of less than 1 µm/s is highlighted. Each population was analysed using a Cramér-

von Mises Test to detect any shift in the population distribution towards lower speed. Percentages are marked with an asterisks when that shift was significant (*$p > 0.05$).

1102 **SUPPLEMENTARY FILES**

1103 **Supplementary File 1. Primers used in this study.**

1104 **Supplementary File 2. Plasmid maps.** Genbank files of pTB102, pTB104, pTB105, pTB106 and
1105 pTB107.

1106 **Supplementary File 3. A protocol for AsCas12a-mediated transfection of CBE sgRNA**
1107 **expression cassettes.** Step-by-step protocol includes guidelines for PCR amplification of donor DNA
1108 and Cas12a crRNA template DNA, as well as preparations for transfection.

1109 **Supplementary File 4. Analysis of small-scale loss-of-function screen.** The analysis file contains
1110 raw and normalized amplicon sequencing counts for each sgRNA subjected to the screen, along with
1111 the ratio analysis shown in Figure 5.

1112 **Source code 1. Novel scoring for CBE sgRNA sorting.** Source code for CBE sgRNA scoring
1113 described above. The updated data sets can be accessed at http://www.leishbaseedit.net/. The
1114 source code for the guide scoring has been uploaded to
1115 https://github.com/ElisabethMeiser/Collaboration_Beneke_Meiser.

1116 **Source data 1. Raw DNA images of Figure 2 S1B and E.** Details as described in Figure 2 S1.

1117 **Source data 2. Raw DNA images of Figure 6B.** Details as described in Figure 6.

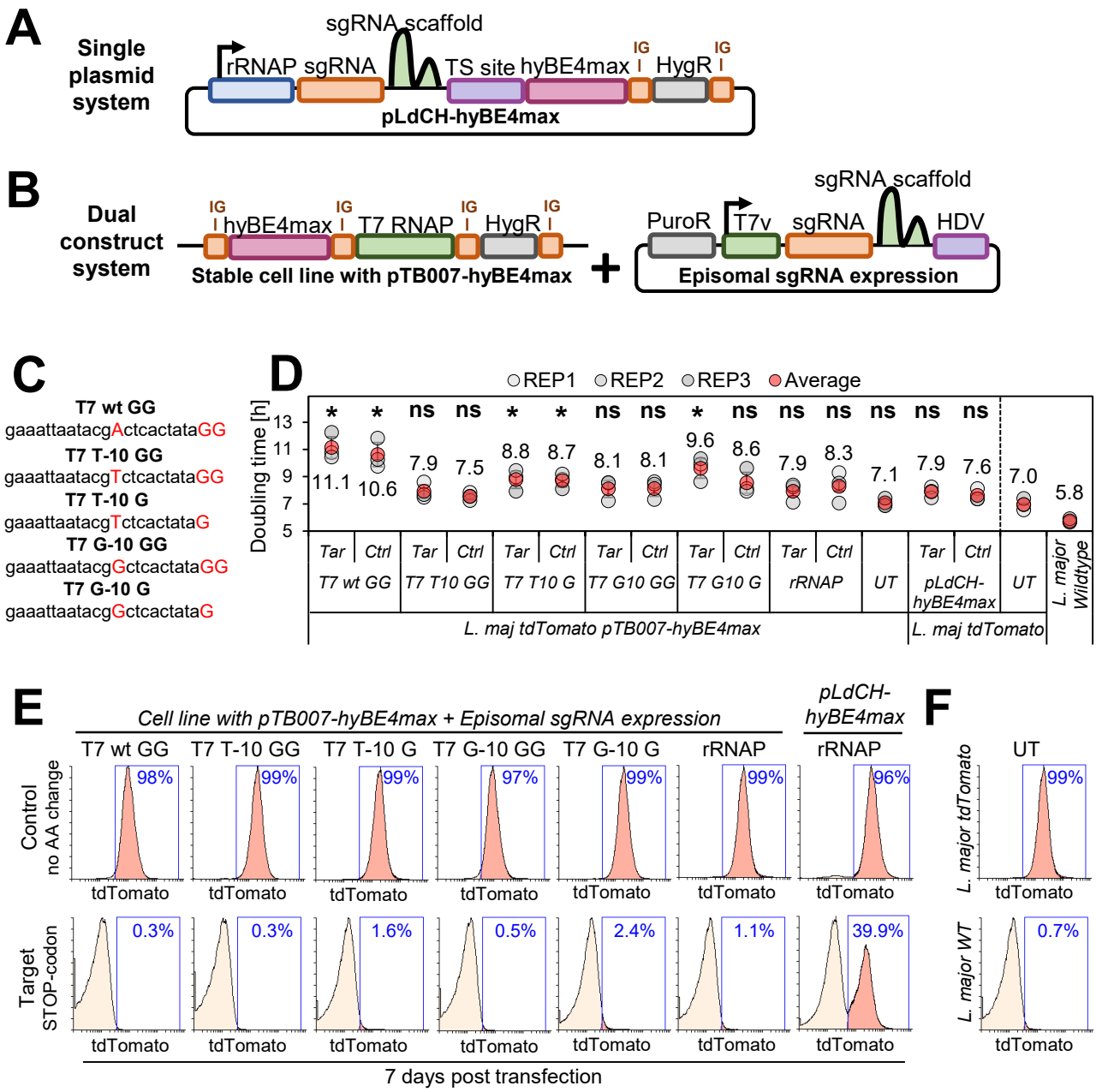
A
Single plasmid system
sgRNA scaffold
rRNAP sgRNA
TS site hyBE4max
IG
HygR
IG
pLdCH-hyBE4max
B
Dual construct system
IG
hyBE4max
IG
T7 RNAP
IG
HygR
IG
Stable cell line with pTB007-hyBE4max
+
sgRNA scaffold
PuroR
T7v
sgRNA
HDV
Episomal sgRNA expression
C
T7 wt GG
gaaattaatacgActcactataGG
T7 T-10 GG
gaaattaatacgTctcactataGG
T7 T-10 G
gaaattaatacgTctcactataG
T7 G-10 GG
gaaattaatacgGctcactataGG
T7 G-10 G
gaaattaatacgGctcactataG
D
REP1
REP2
REP3
Average
Doubling time [h]
13
11
9
7
5
* * ns ns * * ns ns * ns ns ns ns ns ns
11.1
10.6
7.9
7.5
8.8
8.7
8.1
8.1
9.6
8.6
7.9
8.3
7.1
7.9
7.6
7.0
5.8
Tar Ctrl Tar Ctrl Tar Ctrl Tar Ctrl Tar Ctrl Tar Ctrl
T7 wt GG
T7 T10 GG
T7 T10 G
T7 G10 GG
T7 G10 G
rRNAP
UT
pLdCH-hyBE4max
UT
L. major Wildtype
L. maj tdTomato pTB007-hyBE4max
L. maj tdTomato
E
Cell line with pTB007-hyBE4max + Episomal sgRNA expression
pLdCH-hyBE4max
T7 wt GG
T7 T-10 GG
T7 T-10 G
T7 G-10 GG
T7 G-10 G
rRNAP
rRNAP
Control no AA change
98%
99%
99%
97%
99%
99%
96%
Target STOP-codon
0.3%
0.3%
1.6%
0.5%
2.4%
1.1%
39.9%
tdTomato
7 days post transfection
F
UT
L. major tdTomato
99%
L. major WT
0.7%

Figure 1

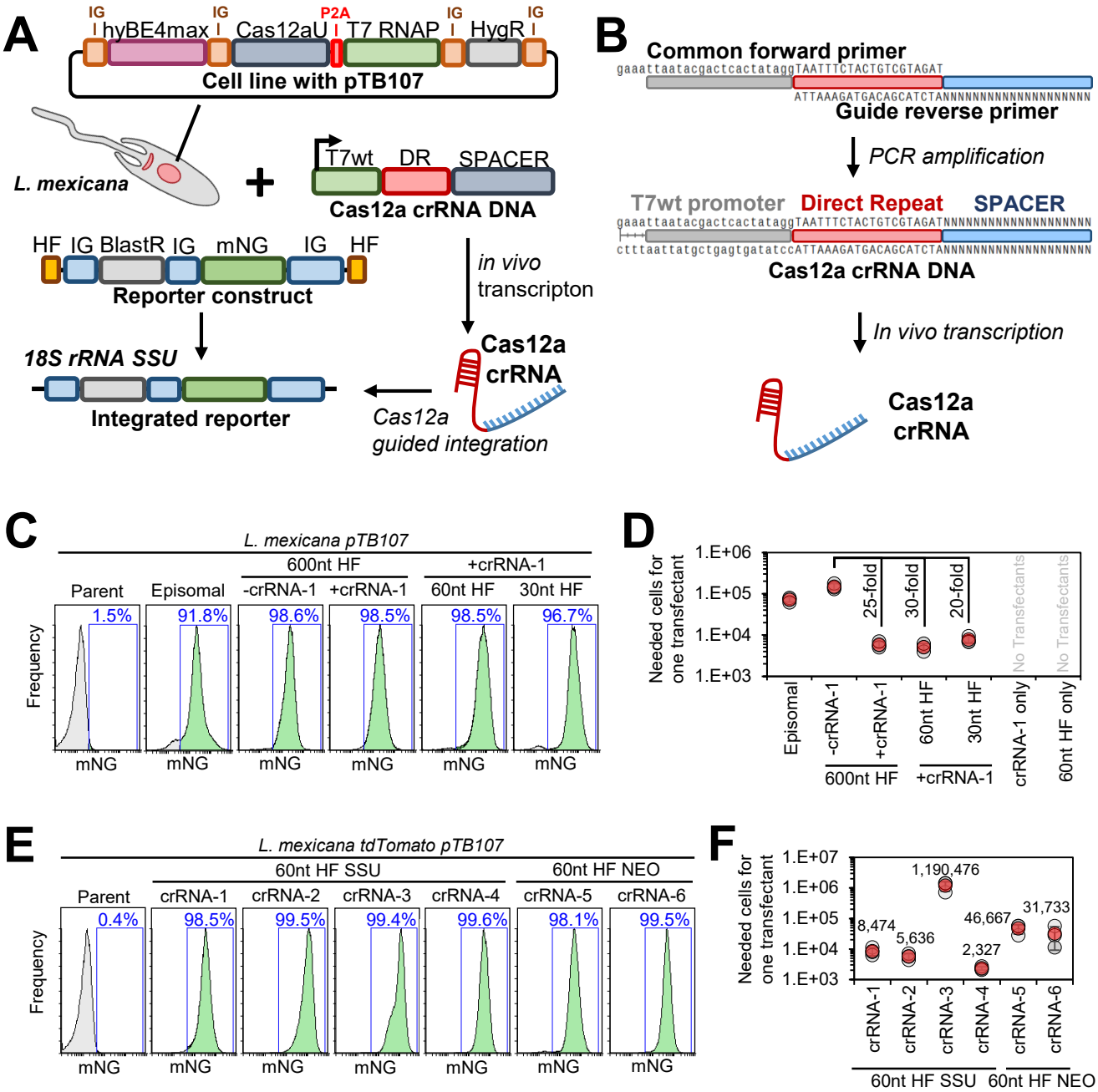
A
IG
hyBE4max
IG
Cas12aU
P2A
T7 RNAP
IG
HygR
IG
Cell line with pTB107
L. mexicana
T7wt
DR
SPACER
Cas12a crRNA DNA
HF IG BlastR IG mNG IG HF
Reporter construct
in vivo transcripton
18S rRNA SSU
Integrated reporter
Cas12a crRNA
Cas12a guided integration
B
Common forward primer
gaaattaatacgactcactataggTAATTTCTACTGTCGTAGAT
ATTAAAGATGACAGCATCTANNNNNNNNNNNNNNNNNNNN
Guide reverse primer
PCR amplification
T7wt promoter
Direct Repeat
SPACER
gaaattaatacgactcactataggTAATTTCTACTGTCGTAGATNNNNNNNNNNNNNNNNNNNN
ctttaattatgctgagtgatatccATTAAAGATGACAGCATCTANNNNNNNNNNNNNNNNNNNN
Cas12a crRNA DNA
In vivo transcription
Cas12a crRNA
C
L. mexicana pTB107
600nt HF
+crRNA-1
Parent
Episomal
-crRNA-1
+crRNA-1
60nt HF
30nt HF
1.5%
91.8%
98.6%
98.5%
98.5%
96.7%
Frequency
mNG
D
Needed cells for one transfectant
1.E+06
1.E+05
1.E+04
1.E+03
25-fold
30-fold
20-fold
No Transfectants
No Transfectants
Episomal
-crRNA-1
+crRNA-1
60nt HF
30nt HF
crRNA-1 only
60nt HF only
600nt HF
+crRNA-1
E
L. mexicana tdTomato pTB107
60nt HF SSU
60nt HF NEO
Parent
crRNA-1
crRNA-2
crRNA-3
crRNA-4
crRNA-5
crRNA-6
0.4%
98.5%
99.5%
99.4%
99.6%
98.1%
99.5%
Frequency
mNG
F
Needed cells for one transfectant
1.E+07
1.E+06
1.E+05
1.E+04
1.E+03
1,190,476
8,474
5,636
2,327
46,667
31,733
crRNA-1
crRNA-2
crRNA-3
crRNA-4
crRNA-5
crRNA-6
60nt HF SSU
60nt HF NEO

Figure 2

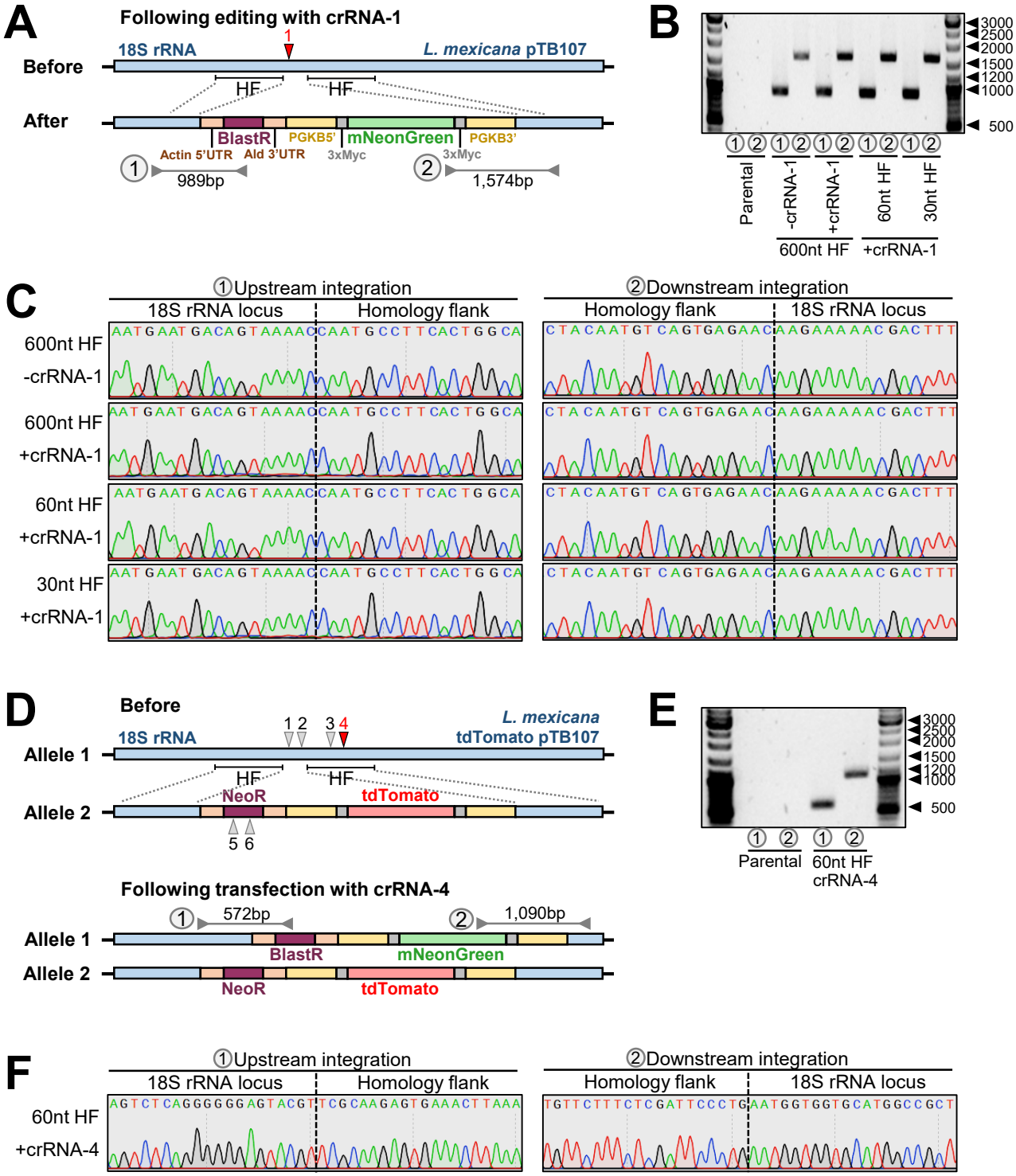
A
Following editing with crRNA-1
18S rRNA
L. mexicana pTB107
Before
After
HF
HF
BlastR
PGKB5'
mNeonGreen
PGKB3'
Actin 5'UTR
Ald 3'UTR
3xMyc
3xMyc
989bp
1,574bp
B
3000
2500
2000
1500
1200
1000
500
Parental
-crRNA-1
+crRNA-1
60nt HF
30nt HF
600nt HF
+crRNA-1
C
①Upstream integration
②Downstream integration
18S rRNA locus
Homology flank
Homology flank
18S rRNA locus
600nt HF
-crRNA-1
600nt HF
+crRNA-1
60nt HF
+crRNA-1
30nt HF
+crRNA-1
D
Before
L. mexicana
tdTomato pTB107
18S rRNA
Allele 1
Allele 2
HF
HF
NeoR
tdTomato
Following transfection with crRNA-4
572bp
1,090bp
Allele 1
Allele 2
BlastR
mNeonGreen
NeoR
tdTomato
E
3000
2500
2000
1500
1200
1000
500
Parental
60nt HF
crRNA-4
F
①Upstream integration
②Downstream integration
18S rRNA locus
Homology flank
Homology flank
18S rRNA locus
60nt HF
+crRNA-4

Figure 2 S1

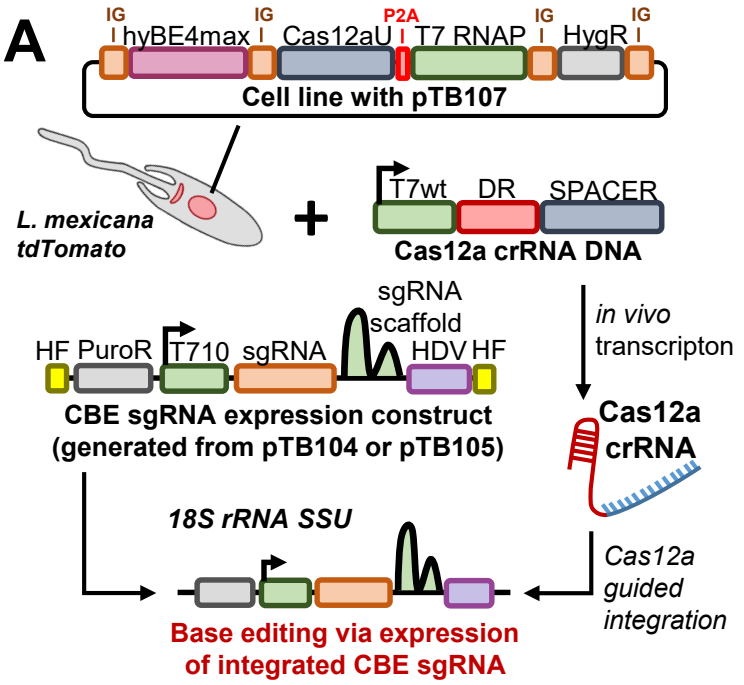
A
IG
hyBE4max
IG
Cas12aU
P2A
T7 RNAP
IG
HygR
IG
Cell line with pTB107
L. mexicana
tdTomato
T7wt
DR
SPACER
Cas12a crRNA DNA
sgRNA
scaffold
HF PuroR
T710
sgRNA
HDV HF
CBE sgRNA expression construct
(generated from pTB104 or pTB105)
in vivo
transcripton
Cas12a
crRNA
18S rRNA SSU
Cas12a
guided
integration
Base editing via expression
of integrated CBE sgRNA

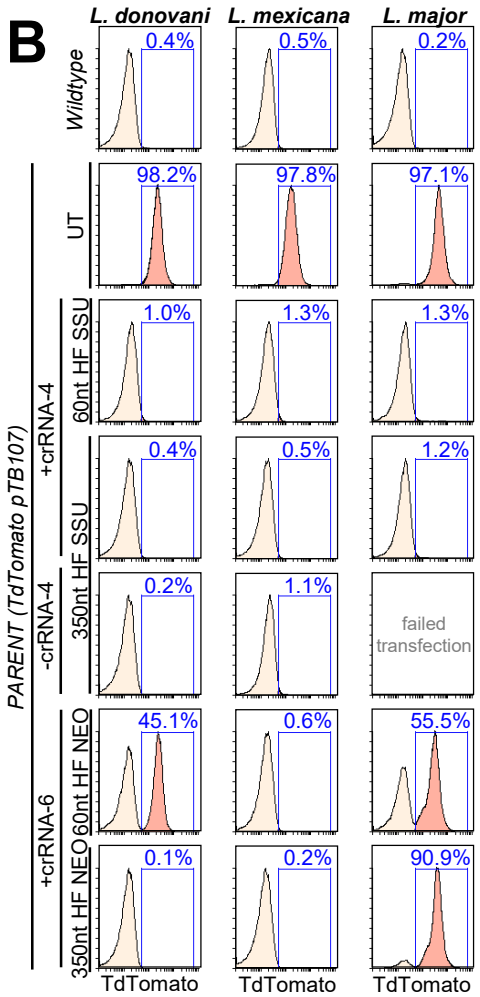
B
L. donovani
L. mexicana
L. major
Wildtype
0.4%
0.5%
0.2%
PARENT (TdTomato pTB107)
UT
98.2%
97.8%
97.1%
+crRNA-4
60nt HF SSU
1.0%
1.3%
1.3%
350nt HF SSU
0.4%
0.5%
1.2%
-crRNA-4
350nt HF SSU
0.2%
1.1%
failed
transfection
+crRNA-6
60nt HF NEO
45.1%
0.6%
55.5%
350nt HF NEO
0.1%
0.2%
90.9%
TdTomato
TdTomato
TdTomato

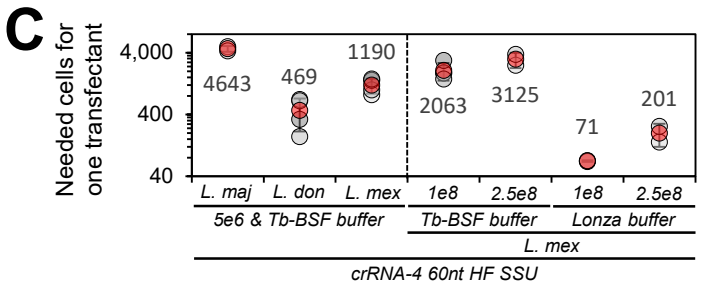
C
Needed cells for
one transfectant
4,000
400
40
4643
469
1190
2063
3125
71
201
L. maj
L. don
L. mex
1e8
2.5e8
1e8
2.5e8
5e6 & Tb-BSF buffer
Tb-BSF buffer
Lonza buffer
L. mex
crRNA-4 60nt HF SSU

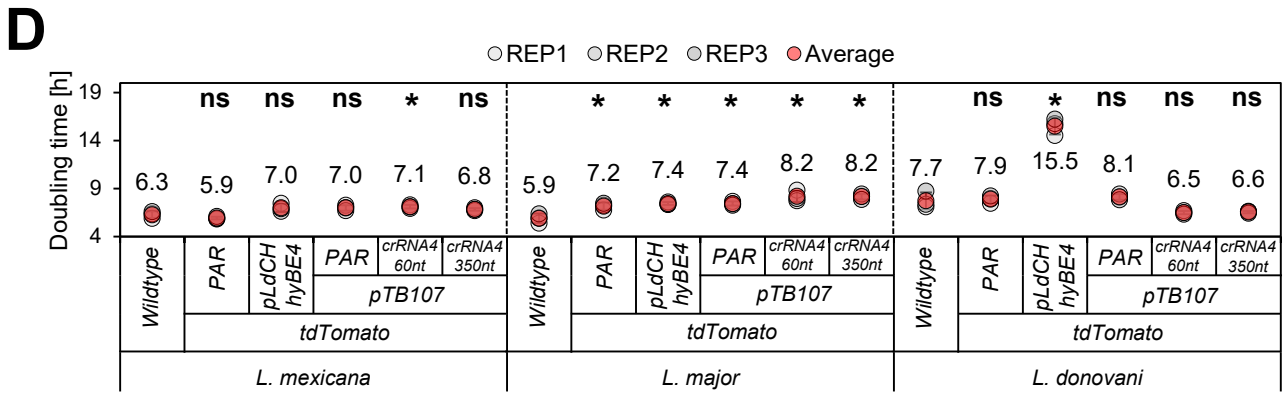
D
REP1
REP2
REP3
Average
Doubling time [h]
19
14
9
4
ns
ns
ns
*
ns
6.3
5.9
7.0
7.0
7.1
6.8
*
*
*
*
*
5.9
7.2
7.4
7.4
8.2
8.2
ns
*
ns
ns
ns
7.7
7.9
15.5
8.1
6.5
6.6
Wildtype
PAR
pLdCH hyBE4
PAR
crRNA4 60nt
crRNA4 350nt
pTB107
tdTomato
L. mexicana
L. major
L. donovani

Figure 3

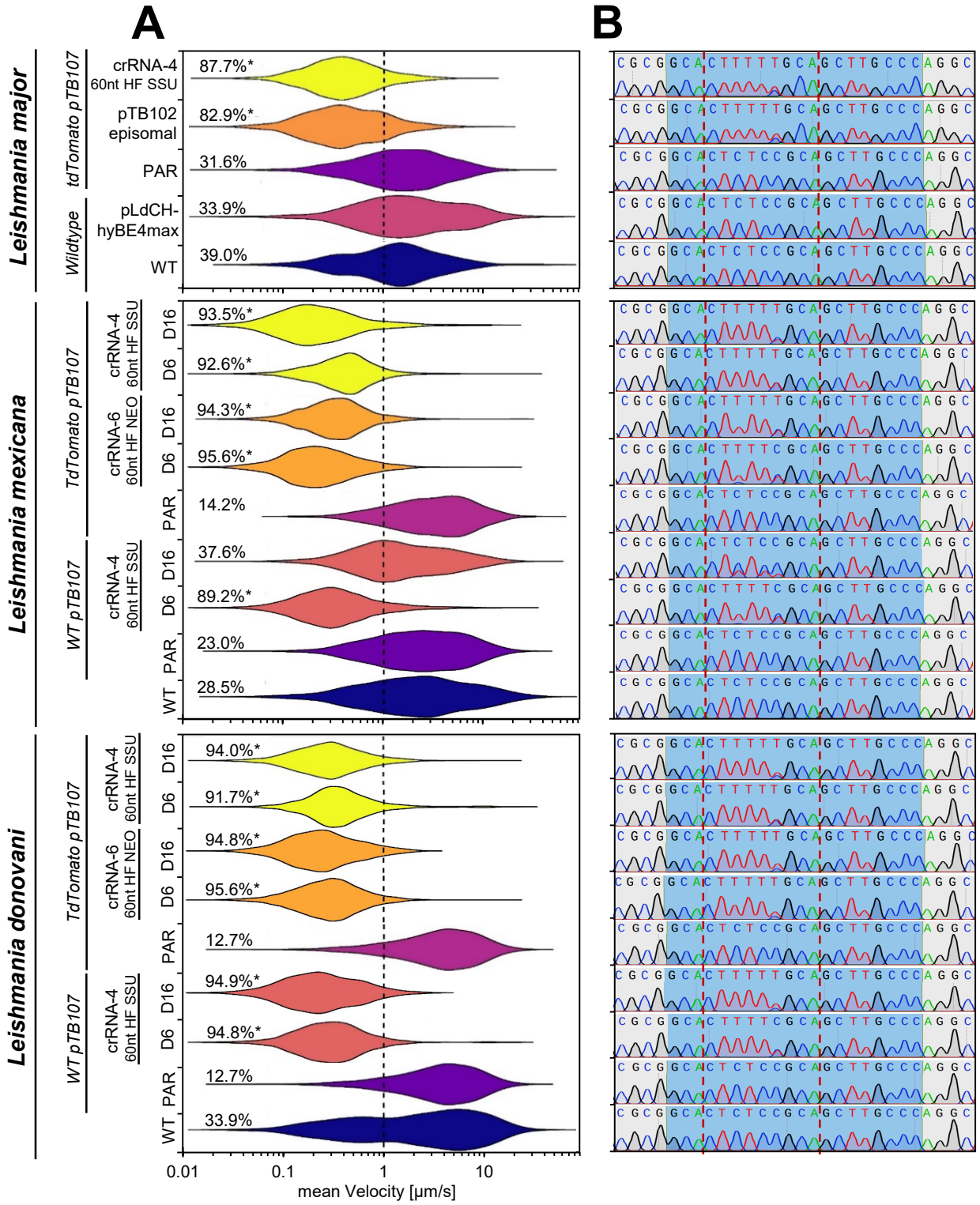
A
B
Leishmania major
tdTomato pTB107
crRNA-4
60nt HF SSU
87.7%*
pTB102
episomal
82.9%*
PAR
31.6%
Wildtype
pLdCH-
hyBE4max
33.9%
WT
39.0%
Leishmania mexicana
TdTomato pTB107
crRNA-4
60nt HF SSU
D16
93.5%*
D6
92.6%*
crRNA-6
60nt HF NEO
D16
94.3%*
D6
95.6%*
PAR
14.2%
WT pTB107
crRNA-4
60nt HF SSU
D16
37.6%
D6
89.2%*
PAR
23.0%
WT
28.5%
Leishmania donovani
TdTomato pTB107
crRNA-4
60nt HF SSU
D16
94.0%*
D6
91.7%*
crRNA-6
60nt HF NEO
D16
94.8%*
D6
95.6%*
PAR
12.7%
WT pTB107
crRNA-4
60nt HF SSU
D16
94.9%*
D6
94.8%*
PAR
12.7%
WT
33.9%
0.01
0.1
1
10
mean Velocity [µm/s]

Figure 4

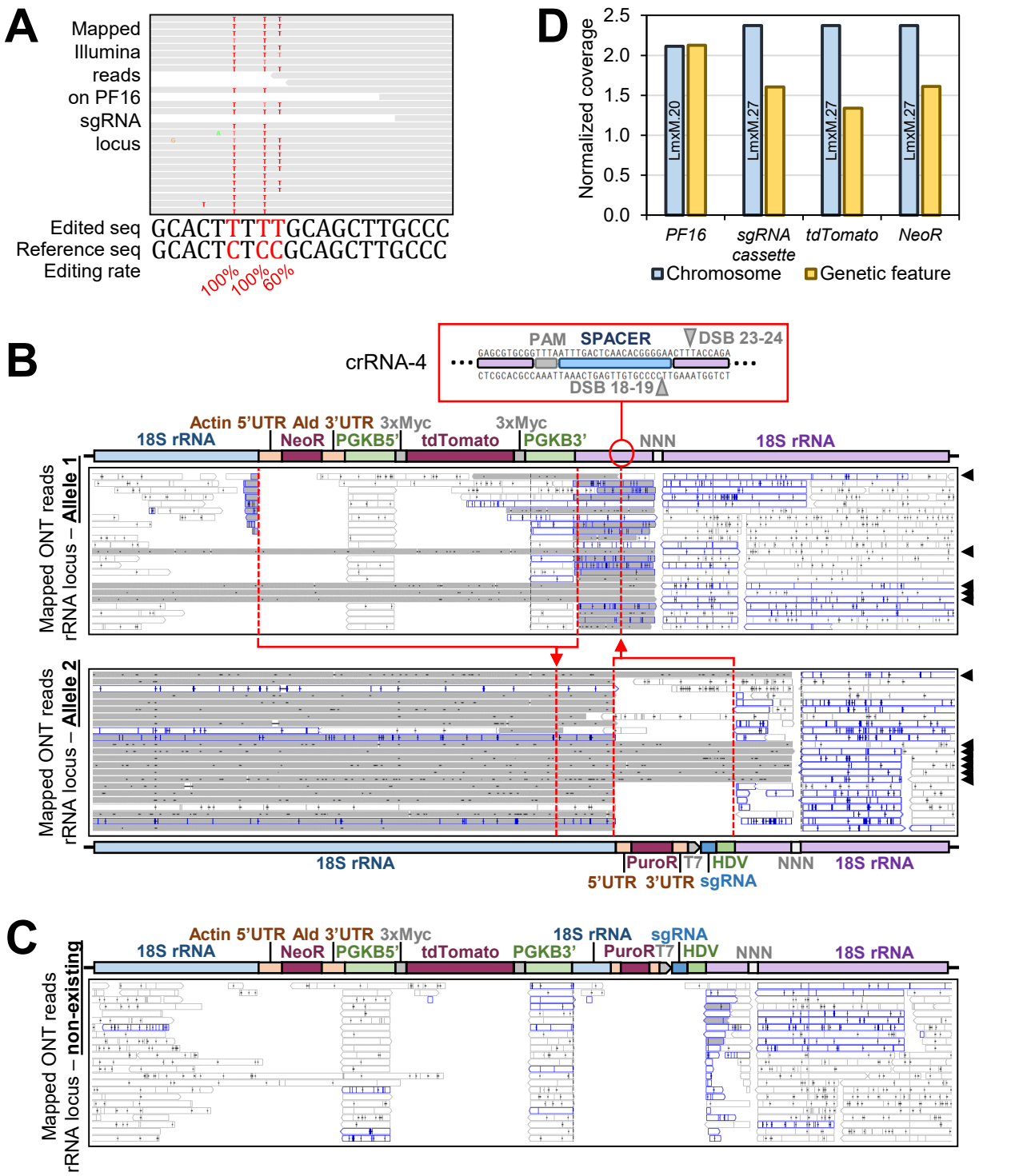
A
Mapped Illumina reads on PF16 sgRNA locus
Edited seq GCACTTTTTGCAGCTTGCCC
Reference seq GCACTCTCCGCAGCTTGCCC
Editing rate
100% 100% 60%
D
Normalized coverage
2.5
2.0
1.5
1.0
0.5
0.0
LmxM.20
LmxM.27
LmxM.27
LmxM.27
PF16
sgRNA cassette
tdTomato
NeoR
Chromosome
Genetic feature
B
crRNA-4
PAM
SPACER
DSB 23-24
DSB 18-19
Actin 5'UTR
Ald 3'UTR
3xMyc
3xMyc
18S rRNA
NeoR
PGKB5'
tdTomato
PGKB3'
NNN
18S rRNA
Mapped ONT reads rRNA locus – Allele 1
Mapped ONT reads rRNA locus – Allele 2
18S rRNA
PuroR
T7
HDV
NNN
18S rRNA
5'UTR
3'UTR
sgRNA
C
Mapped ONT reads rRNA locus – non-existing
Actin 5'UTR
Ald 3'UTR
3xMyc
18S rRNA
sgRNA
18S rRNA
NeoR
PGKB5'
tdTomato
PGKB3'
PuroR
T7
HDV
NNN
18S rRNA

Figure 4 S1

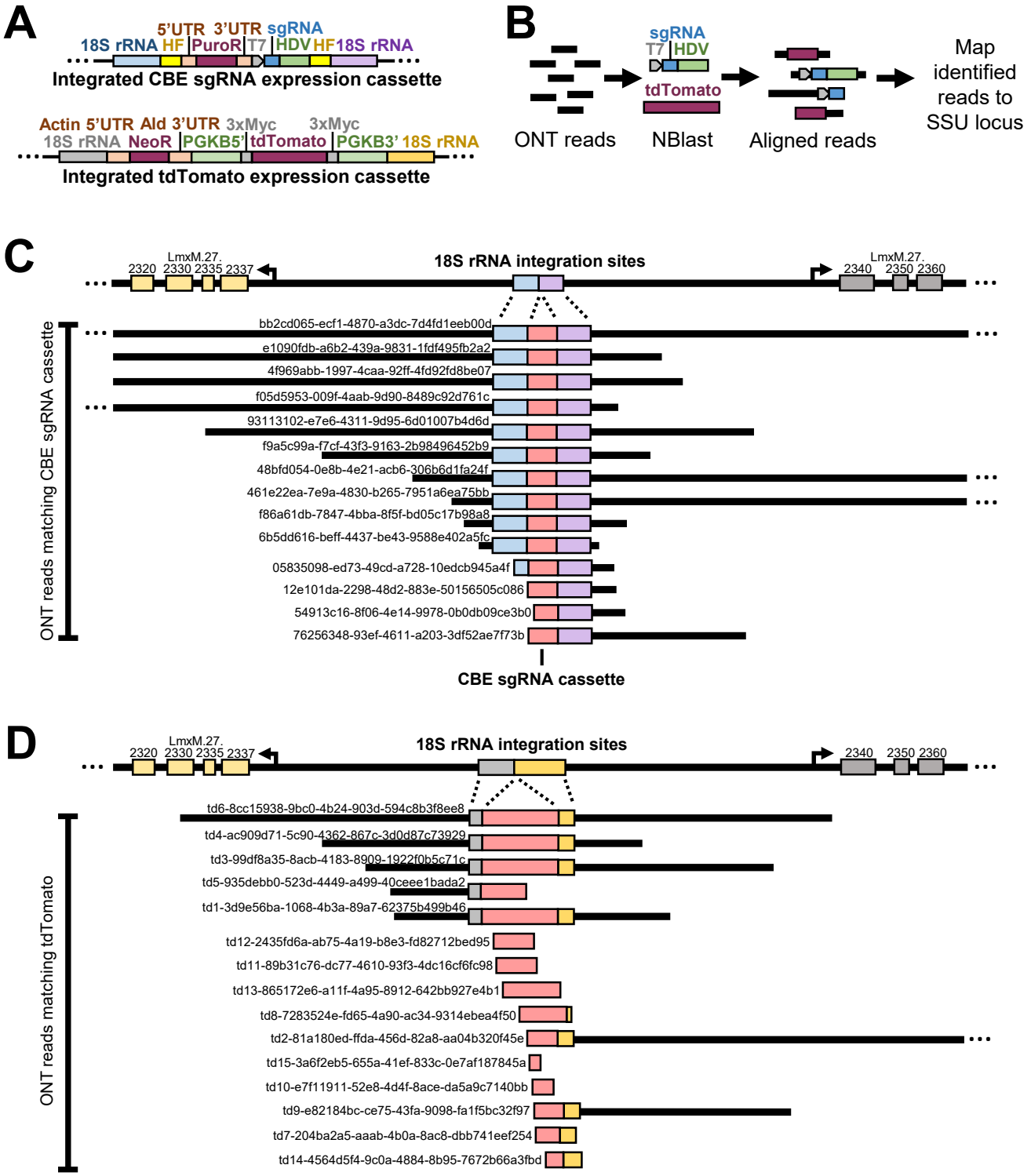
A
5'UTR 3'UTR sgRNA
18S rRNA HF PuroR T7 HDV HF 18S rRNA
Integrated CBE sgRNA expression cassette
Actin 5'UTR Ald 3'UTR 3xMyc 3xMyc
18S rRNA NeoR PGKB5' tdTomato PGKB3' 18S rRNA
Integrated tdTomato expression cassette
B
sgRNA
T7 HDV
tdTomato
ONT reads
NBlast
Aligned reads
Map identified reads to SSU locus
C
LmxM.27.
2320 2330 2335 2337
18S rRNA integration sites
LmxM.27.
2340 2350 2360
ONT reads matching CBE sgRNA cassette
bb2cd065-ecf1-4870-a3dc-7d4fd1eeb00d
e1090fdb-a6b2-439a-9831-1fdf495fb2a2
4f969abb-1997-4caa-92ff-4fd92fd8be07
f05d5953-009f-4aab-9d90-8489c92d761c
93113102-e7e6-4311-9d95-6d01007b4d6d
f9a5c99a-f7cf-43f3-9163-2b98496452b9
48bfd054-0e8b-4e21-acb6-306b6d1fa24f
461e22ea-7e9a-4830-b265-7951a6ea75bb
f86a61db-7847-4bba-8f5f-bd05c17b98a8
6b5dd616-beff-4437-be43-9588e402a5fc
05835098-ed73-49cd-a728-10edcb945a4f
12e101da-2298-48d2-883e-50156505c086
54913c16-8f06-4e14-9978-0b0db09ce3b0
76256348-93ef-4611-a203-3df52ae7f73b
CBE sgRNA cassette
D
LmxM.27.
2320 2330 2335 2337
18S rRNA integration sites
2340 2350 2360
ONT reads matching tdTomato
td6-8cc15938-9bc0-4b24-903d-594c8b3f8ee8
td4-ac909d71-5c90-4362-867c-3d0d87c73929
td3-99df8a35-8acb-4183-8909-1922f0b5c71c
td5-935debb0-523d-4449-a499-40ceee1bada2
td1-3d9e56ba-1068-4b3a-89a7-62375b499b46
td12-2435fd6a-ab75-4a19-b8e3-fd82712bed95
td11-89b31c76-dc77-4610-93f3-4dc16cf6fc98
td13-865172e6-a11f-4a95-8912-642bb927e4b1
td8-7283524e-fd65-4a90-ac34-9314ebea4f50
td2-81a180ed-ffda-456d-82a8-aa04b320f45e
td15-3a6f2eb5-655a-41ef-833c-0e7af187845a
td10-e7f11911-52e8-4d4f-8ace-da5a9c7140bb
td9-e82184bc-ce75-43fa-9098-fa1f5bc32f97
td7-204ba2a5-aaab-4b0a-8ac8-dbb741eef254
td14-4564d5f4-9c0a-4884-8b95-7672b66a3fbd

Figure 4 S2

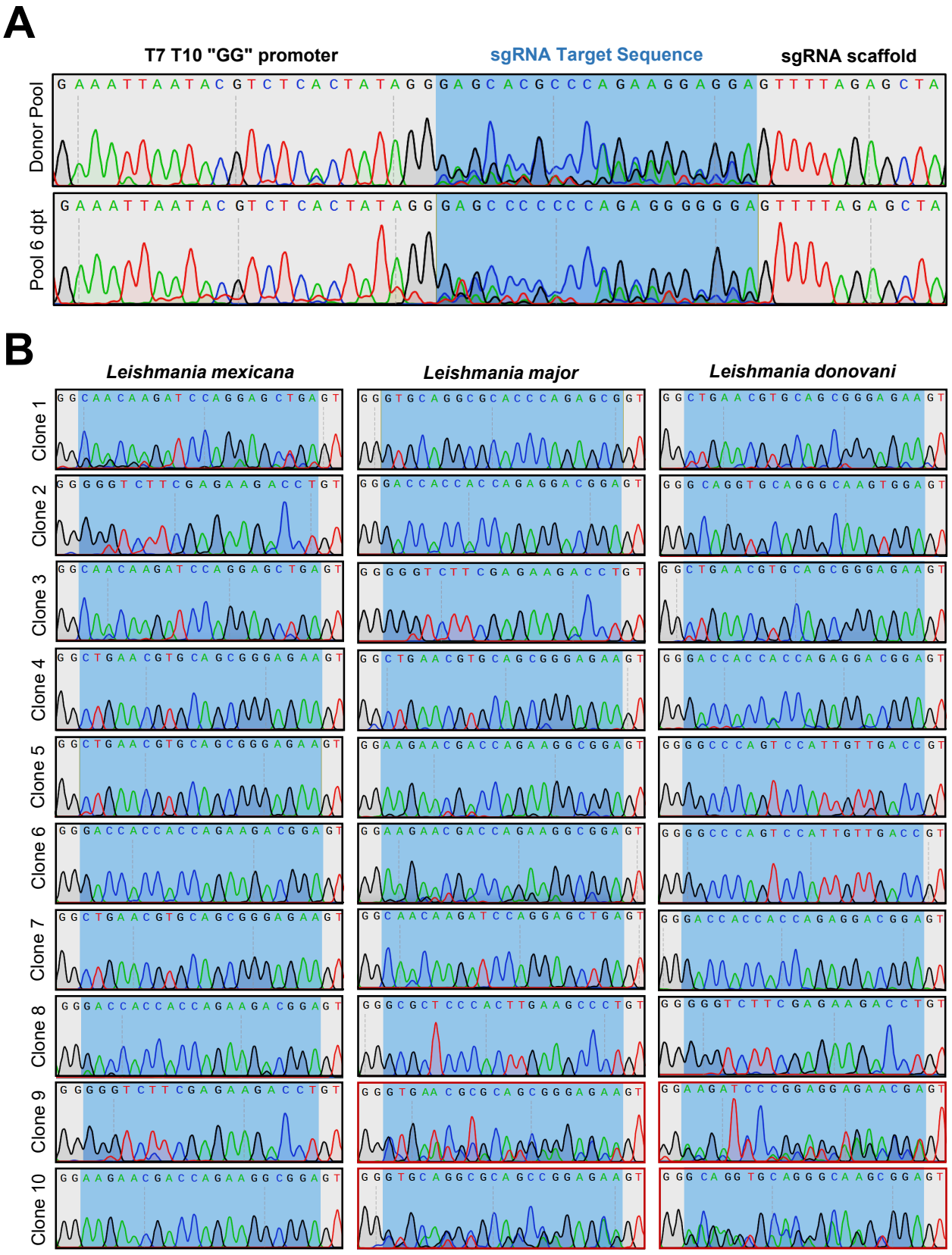
A
T7 T10 "GG" promoter
sgRNA Target Sequence
sgRNA scaffold
Donor Pool
Pool 6 dpt
B
Leishmania mexicana
Leishmania major
Leishmania donovani
Clone 1
Clone 2
Clone 3
Clone 4
Clone 5
Clone 6
Clone 7
Clone 8
Clone 9
Clone 10

Figure 4 S3

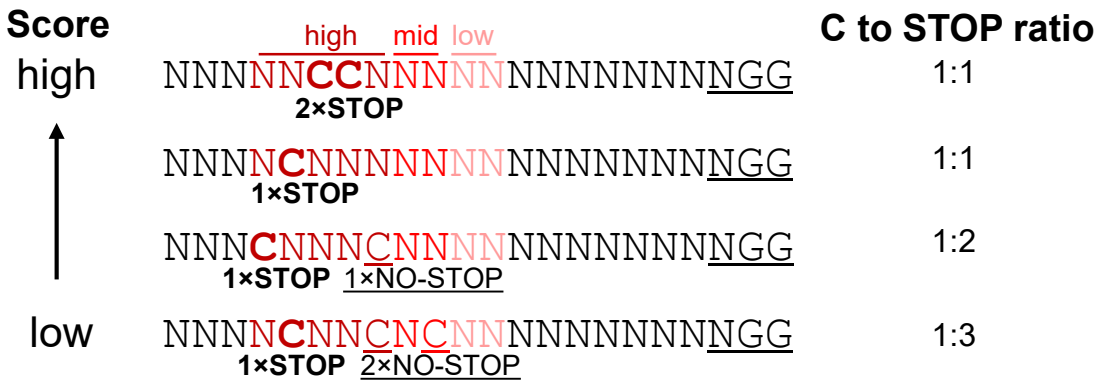
Score
high
low
high
mid
low
C to STOP ratio
NNNNNCCNNNNNNNNNNNNNNNGG
2×STOP
1:1
NNNNCNNNNNNNNNNNNNNNNGG
1×STOP
1:1
NNNCNNNCNNNNNNNNNNNNNGG
1×STOP
1×NO-STOP
1:2
NNNNCNNCNCNNNNNNNNNNNGG
1×STOP
2×NO-STOP
1:3

Figure 4 S4

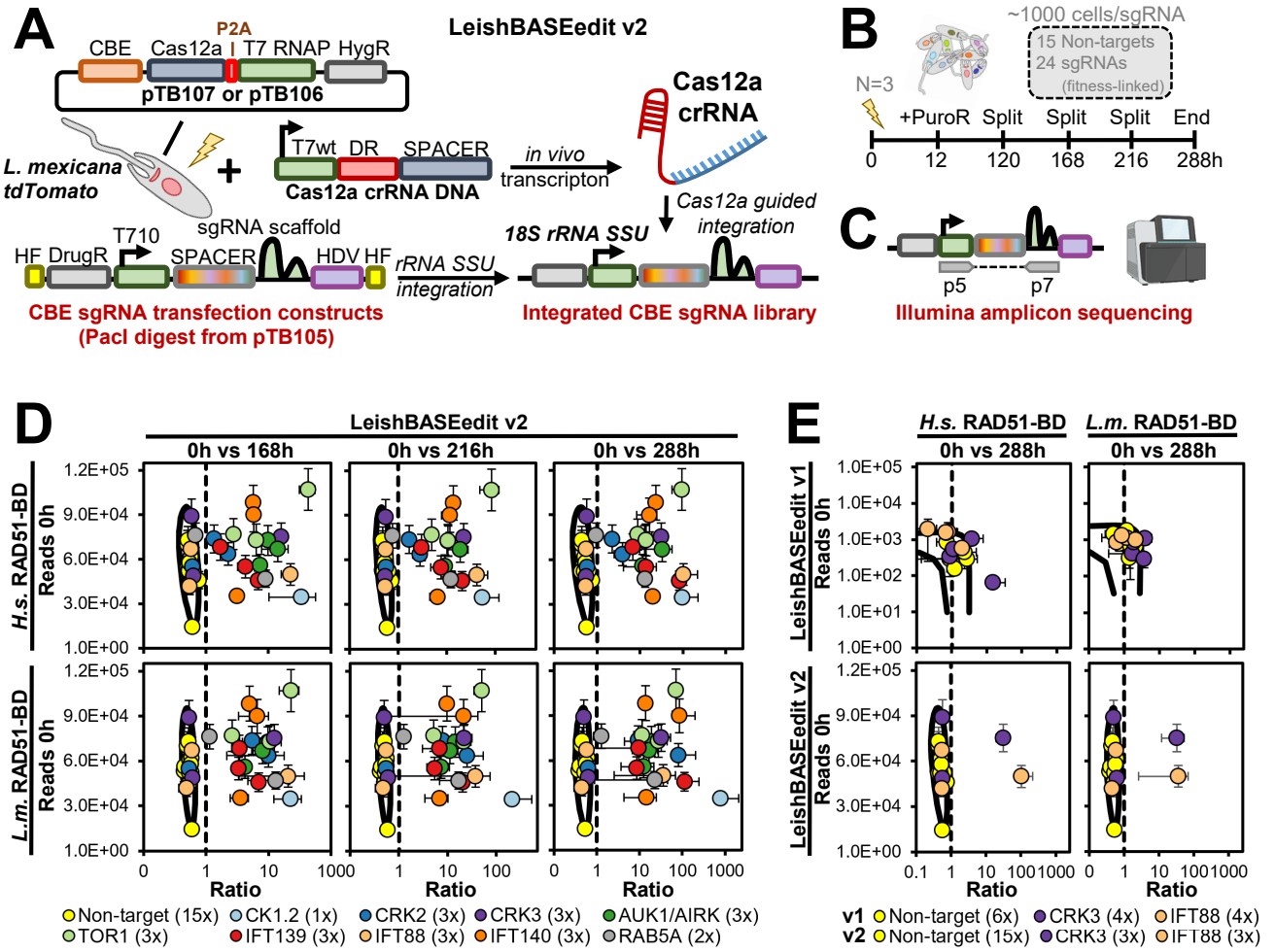
A
LeishBASEedit v2
P2A
CBE
Cas12a
T7 RNAP
HygR
pTB107 or pTB106
L. mexicana tdTomato
T7wt
DR
SPACER
Cas12a crRNA DNA
in vivo transcripton
Cas12a crRNA
Cas12a guided integration
18S rRNA SSU
sgRNA scaffold
T710
HF
DrugR
SPACER
HDV
HF
rRNA SSU integration
CBE sgRNA transfection constructs (PacI digest from pTB105)
Integrated CBE sgRNA library
B
~1000 cells/sgRNA
15 Non-targets
24 sgRNAs
(fitness-linked)
N=3
+PuroR
Split
Split
Split
End
0
12
120
168
216
288h
C
p5
p7
Illumina amplicon sequencing
D
LeishBASEedit v2
0h vs 168h
0h vs 216h
0h vs 288h
H.s. RAD51-BD
L.m. RAD51-BD
Reads 0h
Ratio
Non-target (15x)
CK1.2 (1x)
CRK2 (3x)
CRK3 (3x)
AUK1/AIRK (3x)
TOR1 (3x)
IFT139 (3x)
IFT88 (3x)
IFT140 (3x)
RAB5A (2x)
E
H.s. RAD51-BD
L.m. RAD51-BD
0h vs 288h
LeishBASEedit v1
LeishBASEedit v2
Reads 0h
Ratio
v1 Non-target (6x)
CRK3 (4x)
IFT88 (4x)
v2 Non-target (15x)
CRK3 (3x)
IFT88 (3x)

Figure 5

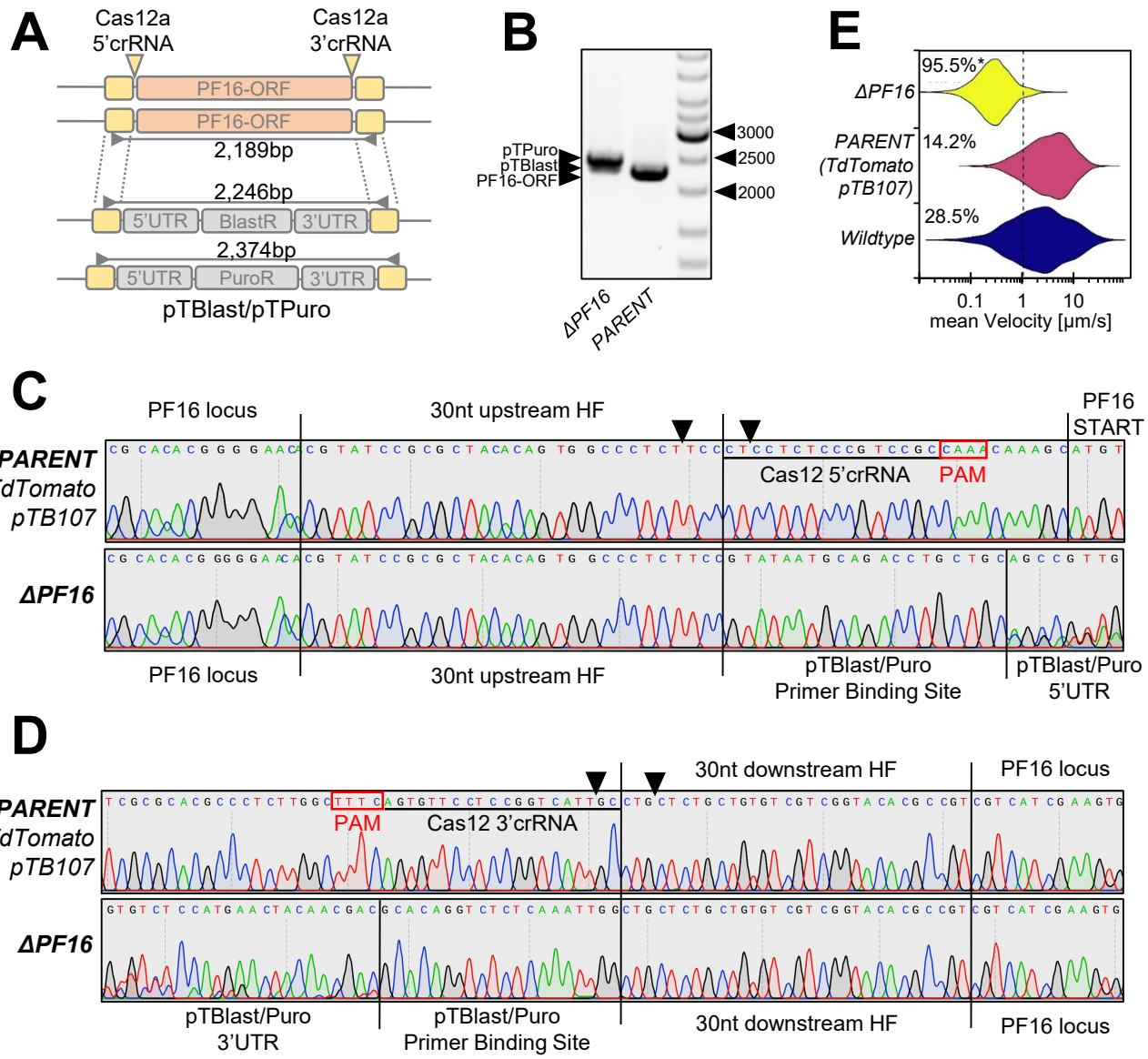
A
Cas12a
5'crRNA
Cas12a
3'crRNA
PF16-ORF
PF16-ORF
2,189bp
2,246bp
5'UTR
BlastR
3'UTR
2,374bp
5'UTR
PuroR
3'UTR
pTBlast/pTPuro
B
pTPuro
pTBlast
PF16-ORF
3000
2500
2000
ΔPF16
PARENT
E
95.5%*
ΔPF16
PARENT
(TdTomato
pTB107)
14.2%
28.5%
Wildtype
0.1
1
10
mean Velocity [µm/s]
C
PF16 locus
30nt upstream HF
PF16
START
PARENT
TdTomato
pTB107
Cas12 5'crRNA
PAM
ΔPF16
PF16 locus
30nt upstream HF
pTBlast/Puro
Primer Binding Site
pTBlast/Puro
5'UTR
D
30nt downstream HF
PF16 locus
PARENT
TdTomato
pTB107
PAM
Cas12 3'crRNA
ΔPF16
pTBlast/Puro
3'UTR
pTBlast/Puro
Primer Binding Site
30nt downstream HF
PF16 locus

Figure 6